Energy & Buildings 309 (2024) 114066

Contents lists available at ScienceDirect

Energy & Buildings

journal homepage: www.elsevier.com/locate/enbuild

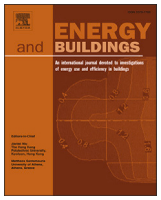

Long-term operational planning for flexible residential buildings with seasonal storage and capacity-based grid tariffs

Kasper Emil Thorvaldsen [a,b,*], Stian Backe [a], Hossein Farahmand [b]

[a] SINTEF Energy Research, Dept. of Energy Systems, Trondheim, Norway
[b] Department of Electric Energy, Norwegian University of Science and Technology, Trondheim, Norway

ARTICLE INFO

Keywords:
Demand-side management
Capacity-based grid tariff
Seasonal thermal energy storage
Seasonal flexibility
Operational planning
Stochastic dynamic programming
Future cost curves

ABSTRACT

When performing operation of the energy system in a building, it is difficult to accurately represent the uncertain long-term objectives in the short-term window, and the correlation between long-term objectives. This work investigates a strategic modelling framework for representing long-term incentives during short-term operational planning for an energy system within flexible buildings. Multi-stage backwards Stochastic Dynamic Programming (SDP) is used to decompose the yearly operational problem into smaller stages, and create long-term cost curves that captures the cost of adjusting long-term price signals, which in this work considers seasonal thermal energy storage and recurring monthly capacity-based grid tariff costs. The proposed method is analyzed for a flexible realistic Norwegian building located in Southern Norway, where the influence both price signals have on long-term operational performance is analyzed. Results show that the framework strategically optimizes the long-term seasonal storage together with the recurring monthly grid tariff, complementing each other by using the seasonal storage to reduce peak costs during winter. With both seasonal storage and monthly demand charge, yearly operational costs are reduced by 4.3% compared to only accounting for the grid tariff. Additionally, the operational performance achieved only a 0.9% higher cost compared to yearly simulation with perfect information.

Acronyms

BESS	Battery Energy Storage System
COP	Coefficient Of Performance
EFCCs	Expected Future Cost Curves
EV	Electric Vehicle
HP	Heat Pump
MDP	Markov Decision Process
MPGT	Measured Peak Grid Tariff
PI	Perfect Information
PV	Photovoltaic
SDP	Stochastic Dynamic Programming
SoC	State-of-Charge
STES	Seasonal Thermal Energy Storage

1. Introduction

The roll-out of smart meters for electricity use in buildings and households [1] enables more dynamic interaction with the end users to be implemented. Smart meters provide more opportunities to implement demand response programs, giving better options to reflect the grid operators' cost at the end-user level with more dynamic grid tariffs. Given beneficial demand response programs and grid tariffs, the end users can adjust their consumption pattern to reduce stress on the grid, e.g., time-of-use and real-time prices. Norway has recently implemented a capacity-based grid tariff called measured-peak grid tariff (Measured Peak Grid Tariff (MPGT)) for end users [2,3], also known as demand charge. For residential users, it puts a cost on the average of the three highest single-hour import levels, spread across different days over the course of a month, while for others, it is based on the highest single-hour import level over the month [4], which promotes peak-shaving and an overall flat consumption profile. This work only examines the structure with the highest single-hour import level. The MPGT has already existed in Norway for end users with a high con-

* Corresponding author at: SINTEF Energy Research, Dept. of Energy Systems, Trondheim, Norway.
E-mail address: kasper.thorvaldsen@sintef.no (K.E. Thorvaldsen).

https://doi.org/10.1016/j.enbuild.2024.114066
Received 20 November 2023; Received in revised form 13 February 2024; Accepted 5 March 2024
Available online 7 March 2024

Nomenclature

Index sets

S_g	set of state variables
$\mathcal{T}$	Set of time steps within the day
$L_{x,z}$	Set containing indices for weighting variable γ coupled to discrete point x of state variable SV.
N^P	Set of segments for both state variables
N_0^P	Set of segments for the MPGT state variable
N_1^P	Set of segments for the STES state variable
N_g^S	Set of scenarios for stochastic variables for stage g
S_{MPGT}	Set on stages that initiate a new long-term price signal for the MPGT
$\mathcal{G}$	set of days within the year

Parameters

$\dot{E}^{B,dch}, \dot{E}^{B,ch}$	Discharge/charge capacity for battery	$\frac{kWh}{h}$
$\dot{E}^{Max}$	Maximum EV charging capacity	$\frac{kWh}{h}$
$\dot{E}_t^{STES,in}$	Rated input capacity limit for the STES	$\frac{kWh}{h}$
$\dot{E}_t^{STES,out}$	Rated output capacity limit for the STES	$\frac{kWh}{h}$
$\dot{Q}^{sh}$	Capacity for space heating radiator	$\frac{kWh}{h}$
$\eta_{dch}^B, \eta_{ch}^B$	Discharge/charge efficiency for battery	p.u
η_{ch}^{EV}	EV charging efficiency	p.u
η^{PV}	Total efficiency for PV system	p.u
η^{STES}	Daily losses for the STES	p.u
C^{grid}	Volumetric energy grid tariff for imported energy	$\frac{EUR}{kWh}$
$C_{n,m}^{Future}$	Expected future cost for segment n,m	EUR
A^{PV}	PV system area	m^2
C_i, C_e	Heat capacity for interior and building envelope	$\frac{kWh}{°C}$
C_g^{MPGT}	Marginal monthly cost for MPGT for stages g within P_{List}	
COP^{HP}	Coefficient of performance for the Heat Pump (HP)	p.u
D^{EV}	EV discharge when not connected	kWh
$E^{B,min}, E^{B,max}$	Battery SoC limits	kWh
$E^{EV,min}, E^{EV,max}$	Min/Max EV SoC capacity	kWh
E_{Rated}^{STES}	Rated storage capacity for the STES tank	kWh
E_0^{STES}	Initial state of charge for STES	kWh
P^{HP}	Rated electrical capacity for the HP	$\frac{kWh}{h}$
P_0^{imp}	Initial peak power	$\frac{kWh}{h}$
P_m^{STES}	STES SoC at segment m	kWh
P_n^{imp}	Peak power at point n	$\frac{kWh}{h}$
P_g^{MPGT}	Initial value for the MPGT state variable that ends in stage g within P_{List}	
R_{ie}, R_{eo}	The thermal resistance between the interior-building envelope and building envelope-outdoor area	$\frac{°C}{kWh}$
$T_t^{in,min}, T_t^{in,max}$	Lower/upper interior boundary	°C
VAT	Value added tax for purchase of electricity	p.u

Decision variables

α^{future}	Expected future cost	EUR
β_n	Weighted variable for peak import segment n	
η_m	Weighted variable for STES SoC segment m	
$\gamma_{n,m}$	Weighted variable for (MPGT) and STES State-of-Charge (SoC) segment n,m	
E_t^B	State of charge for Battery for time step t	kWh
E_t^{EV}	State of charge for EV for time step t	kWh
E_t^{STES}	State of charge for STES	kWh
p^{imp}	Peak of imported energy	$\frac{kWh}{h}$
q_t^{sh}	Thermal energy for space heating	$\frac{kWh}{h}$
T_t^{in}, T_t^e	Interior and building envelope temperature	°C
$y_t^{B,ch}, y_t^{B,dch}$	Power to/from the battery for time step t	$\frac{kWh}{h}$
$y_t^{EV,ch}$	Input power to EV for time step t	$\frac{kWh}{h}$
$y_t^{HP,out}$	Output thermal energy from heat pump	$\frac{kWh}{h}$
y_t^{HP}	Input electric power to heat pump	$\frac{kWh}{h}$
y_t^{imp}, y_t^{exp}	Energy imported/exported to building	$\frac{kWh}{h}$
y_t^{PV}	Power produced from Photovoltaic (PV) system	$\frac{kWh}{h}$
$y_t^{STES,in}$	Thermal energy input for Seasonal Thermal Energy Storage (STES)	$\frac{kWh}{h}$
$y_t^{STES,out}$	Thermal energy output from STES	$\frac{kWh}{h}$

Stochastic variables

δ_t^{EV}	Electric Vehicle (EV) connected to building $\{0,1\}$	
C_t^{spot}	Electricity spot price in time step t	$\frac{EUR}{kWh}$
D_t^{el}	Consumer-specific electric load in time step t	kWh
D_t^{WT}	Consumer-specific thermal load in time step t	kWh
I_t^{Irr}	Solar irradiation at building in time step t	$\frac{kWh}{m^2}$
T_t^{out}	Outdoor temperature in time step t	°C

sumption rate (over 100 MWh/year) [5], but is also applied within several member states of the European Union at the end-user level [6]. With the introduction of the MPGT, the use of smart applications like home energy management system to control electricity consumption in the building needs to account for not only the short-term variation in cost, but also the long-term impact from consumption in terms of peak import. Therefore, considering the whole period is essential for cost-optimal operation.

1.1. Monthly measured-peak grid tariff

Recent literature has examined how this long-term MPGT could be taken into account when planning building operation. This literature has only considered an MPGT using the highest single-hour import level over a month of operation. The work in [7] developed an adaptive optimal monthly peak demand limiting strategy for a building with MPGT, where the peak import level was set based on future expectations. This work was extended in [8], where the authors added a trade-off between load predictions and the actual power usage, and managed to achieve monthly peak demand reduction with three different trade-off schemes. However, their schemes either focused on known information or future prediction, and balanced the use of these, not considering both aspects simultaneously when operating. [9] implemented a meta-heuristic approach to balance the real-time pricing and MPGT cost from operation, using a user-defined weighting constant to put a future cost on readjustment of highest monthly peak. However, their method makes the user define what they prioritize with the weighting constant, and therefore the future assumptions are simplified. A strategy framework for finding the optimal MPGT cost was presented in [10], where Expected Future Cost Curves (EFCCs) were created to represent the future value of operation in regards to the MPGT cost. Using stochastic dynamic programming (SDP) in a backwards fashion, the EFCCs helped achieve a 36.1% cost reduction, compared to situations where the MPGT cost was not considered during operation. These results indicate that the use of EFCCs are promising to consider long-term price signals when optimizing day to day operations.

The monthly MPGT cost aims to flatten the consumption profile during a month. However, the MPGT cost can differ based on the seasons. The distribution system operator, Agder Energi Nett in Southern Norway, has different MPGT costs for summer and winter, the cost tripling

in winter compared to the summer in 2019 [4]. Since the electricity grid is more likely to be congested during winter, when the heating demand is noticeably higher, the seasonal variation in MPGT motivates more focus to be put on seasonal flexibility for buildings and end-users. Seasonal flexibility is not only relevant for reducing cost, but also relieving the stress on the grid when it matters the most. Implementing a thermal energy storage system enables the end user to be flexible with their heating demand. Extending this to a seasonal thermal storage (STES) would provide a bigger contribution to the home energy management system, in terms of a monthly MPGT cost. To the authors knowledge, no existing studies have studied the simultaneous consideration of electrical MPGT costs and charging strategy for STES.

1.2. Seasonal thermal flexibility

STES is a flexible asset that enables the operator to store heat over seasons, typically from summer to winter. Different types of STES exist, including hot water tank storage, water-gravel pit storage, and aquifer thermal energy storage [11]. STES enables the storage of excess local solar production, which can increase the performance of renewable sources [12].

When operating an STES, it is important to utilise seasonal variations to store and deliver heat. In [13], an STES was analysed in a simulation model to study the performance of solar district heating systems in the UK, and demonstrated improved efficiency metrics when combined with solar collectors. A combined heat and power plant coupled with an STES was investigated in [14], which indicated more flexibility and higher efficiency during operation. [15] investigated the cost-optimal system for investment and operation using a sector-coupled energy model of Europe. The STES helped to balance long-term and seasonal variations of demand and renewable energy sources.

The operational strategy of an STES fits well with seasonal variation in grid tariff costs, such as the monthly MPGT. Combining an operational strategy for both MPGT and STES would lead to a focus on reducing peak demand during winter when the grid is under the most strain and the presence of renewable solar generation is low. Installing an STES with MPGT would give an additional economic incentive for seasonal storage. In [16], an STES is used for a district heating network to lower the total system cost by storing heat in the summer when several thermal suppliers are available. The results saw a 29% peak generation reduction during winter, and 10% lower operational cost from both the STES and demand-side management. An STES was modelled in [17] to store excess heat from waste incineration to supply heat during winter, with a monthly MPGT cost based on heating import. By using the seasonal storage, and setting peak discharge strategies for the STES, they achieved up to a 39% cost reduction over a year and reduced peak import during winter.

1.3. Contribution

Based on the existing work, there is potential value for a building to use STES to reduce the overall MPGT cost over an operational year. A home energy management system could operate the STES to deal with seasonal variations in heating demand, while also accounting for the seasonal variations of the MPGT. However, the management system would need to account for the long-term impact of operating the STES. To the authors' knowledge, there is no work investigating the long-term strategy for short-term operation of an STES. In addition, there is no work that examines the long-term influence on operating a building with an STES and a monthly MPGT cost.

This work builds on the basis of [10], where SDP is used to develop a strategic modelling framework for a building with a monthly MPGT cost. Such an SDP algorithm can be extended to consider multiple long-term price signals or variables in the EFCCs. In [18], piece-wise linear planes were created for a hydropower system to showcase the dependencies on two state variables on power production: reservoir level and discharge quantity. This method was used in [19] to represent the future value of two reservoirs, where the change in future cost is represented by the combining the change of both variables. Therefore, the EFCCs presented in [10] can be extended to handle multiple state variables, i.e., the MPGT and STES. However, the number of long-term price signals can have operational periods of different horizons. For the SDP framework, the overall horizon accounted for is based on the price signal with the longest period, which in our case is STES, which considers yearly operation. The overall operational strategy needs to make adjustments to the price signals with shorter horizons, like the monthly MPGT, so that their future impact is portrayed accurately. There is a need to create a short-term operational strategy for a system considering multiple long-term price signals with varying operational horizons.

In this paper, we present an extension to the SDP framework in [10], where the generation of the EFCC is extended to allow multiple sets of state variables. This framework will generate future cost curves that consider two sets of state variables, capturing both their impact on operations and their influence on each other. The EFCCs are represented as piece-wise linear planes, determined by two sets of state variables [18]. The SDP framework is applied to an optimization problem representing the energy system within a building, that operates a building with an STES subject to a monthly MPGT cost, which puts a cost on the highest monthly single-hour import level. The optimization problem representing the energy system within a flexible building minimizes cost of operation, considering both the electricity and thermal energy flows. Representation of the energy system is simplified, to focus on how the generated cost curves from the SDP framework manage to capture the long-term economic impact of considering both the seasonal storage and the monthly peak cost.

Our contributions are the following:

- An extension to a general SDP framework applied to a residential building is presented. The EFCCs are made up of two sets of state variables. The operational strategy combines two long-term price signals, capturing their interaction to give a more accurate description on the long-term value of operation. Additionally, the proposed extension includes an algorithm to incorporate multiple price signals with different horizons to the SDP framework. This allows more information on the long-term value of flexibility, with long-term price signals of different characteristics and activation periods during the overall analysis.
- In a numerical case study for a Norwegian residential building, the performance of the EFCC is tested for a year with monthly MPGT and yearly STES operation. We analyse the SDP framework for both price signals, to capture their operational performance and influence on each other over a year. This includes how the monthly MPGT, with seasonal variation in cost, affects the operation and use of STES. The operational performance is compared to cases with perfect information, to showcase the influence of uncertainty within the SDP framework.

The paper progresses as follows. Section 2 introduces the extended SDP framework. The case study used for the analysis is presented in Section 3, while the results and discussion are found in Section 4. The conclusion and future work are given in Section 5.

2. Model description

The primary goal of the proposed SDP framework is to minimize the total electrical operational cost for a residential building over the course of one year. Operation of the building is done by minimizing the current cost of operation, while accounting for the long-term future cost of operation, influenced by the monthly MPGT cost and the STES state-of-charge (SoC). This section details the two parts making up this method; the SDP framework that generates the future cost curves, and the optimization problem used by the SDP framework that details the

energy system in the building. Description of the SDP framework and the structure around it is found in Section 2.1, while the optimization problem is described in Section 2.2.

2.1. Model overview

This work utilizes a long-term operation model for a residential building to find the operational strategy that minimizes the expected cost of operation over the entire planning horizon while accounting for uncertainty. A one-year horizon is considered, as the original problem includes both an STES and a monthly MPGT. To be able to deal with the operational strategy of the STES, whereas decisions during summer and winter are intertwined, the whole year of operation must be considered. As the MPGT only considers a month each time, all twelve independent MPGT costs must be included. Both of these signals are coupled in time, where a short-term here-and-now decision is dependent on the initial condition (historical achievements), and the future consequence. This coupling of historical, current, and future consideration gives the overall problem a dynamic nature. With the presence of uncertainty in the operational decision over the year, the problem can thus be formulated as a multi-stage, multi-scenario optimization problem. Such large problems can be difficult to solve as one big optimization problem, due to the complex nature and size with large scenario trees. Thus, decomposition techniques can be applied, to simplify the overall problem and decrease the computational complexity.

We utilize an SDP framework approach to decompose the overall long-term optimization problem for the residential building. The original problem is here decomposed into several smaller single-stage deterministic optimization problems. Each decomposed problem consist of one specific stage, which can be the operational period of a day or a week, and for a specific scenario within the specific stage. The SDP framework will solve these decomposed problems in a backward procedure, starting at the last stage and calculating towards the first stage. The solution strategy surrounding SDP is presented in Section 2.1.3. The output from the SDP framework is cost curves projecting the future cost of operation, denoted as expected future cost curves (EFCC). These cost curves are generated for each decision stage in the decomposed problem, giving a continuous consideration of the future implications of operation based on what stage you are currently in.

The decision stages themselves are decoupled from each other, with the only dependency they have from each other being the EFCC and the state variables making up the EFCC. The EFCC details the future cost of operation beyond the current decision stage, which is dependent on the value of the state variables. The state variables make up all variables that have a long-term coupling to the original problem, which will be represented through the EFCCs by the SDP framework. For this problem, the state variables include the highest peak import for the MPGT, and the SoC for the STES. The state variables are discretized to describe the EFCC, to capture the change in future strategy based on the change in state variable value.

To couple the decision stages together within the SDP framework, we formulate a set S_g that contains information that is carried over between decision stages g and $g-1$. Within this set lies two subsets; N_g^S contains the indices that define what scenarios are to be analyzed for the decision stage g. Each scenario specify the realized values for the stochastic variables of the overall problem, which is explained more in Section 2.1.1. The set N^P contains a list of indices for the initial values of the state variables that represent the future cost curve. The state variables comprise the discrete number of points for historically achieved peak import P_0^{imp}, and initial SoC for the STES E_0^{STES}. We analyze how the future cost curve follow the change in state variable values. The range, and the number of discrete values for each state variable, provide a good overview and accuracy over the operational strategy throughout the year. The level of detail on the discretized future cost curve, as well as the number of scenarios and stages, creates a trade-off between accuracy and computational time usage, known as the curse of dimensionality, which is explained in [20]. Combining both subsets, all decomposed decision problems that we investigate for decision stage g is defined by both subsets $N_g^S, N^P \subseteq S_g$, with each decomposed decision problem being defined by the scenario $s_g \in N_g^S$, and the initial value of the two state variables $n \in N^P$.

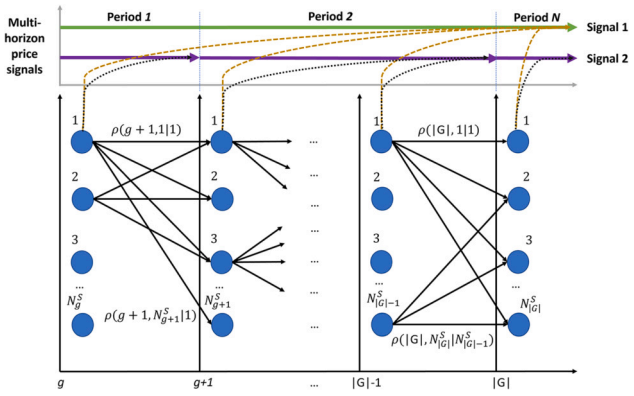

Fig. 1. Illustration of the scenario coupling between stage transition, and the correlation between stages and the multiple price signals. Note that the price signals can be refreshed during the overall horizon.

2.1.1. Stochastic behaviour

The SDP framework enables uncertainty to be included within the analysis, creating strategies that account for stochastic scenarios during operation. This work considers that uncertainty can be put into two categories for building operation: weather effects and user behaviour. To represent this within the SDP framework, the stochastic scenarios can be represented as discrete scenario nodes using a discrete Markov chain. The discrete Markov chain gives discrete scenario nodes for each specific decision stage, and corresponding probabilities for scenario transition between decision stages. With a discrete Markov chain, each decomposed decision problem g would consider N_g^S discrete scenario nodes, where each scenario node contains realized values of the uncertainty considered. Each decomposed optimization problem is represented as a Markov Decision Process (MDP), where the problem is assumed to be memoryless, only considering the current scenario s_g and the probability of the future scenarios $s_{g+1} \in N_g^S$ [21,22]. The only prior information the optimization problem considers is the initial value for the state variables, that is analyzed for multiple discrete values to cover how operation could occur prior. Thus, the decomposed optimization problem only considers the current situation and the weighted outcome of the next future decision stage $g+1$, where the latter is represented by the generated EFCCs. The use of Markov chain to handle the stochastic variables has been performed for SDP within hydropower scheduling, for instance in reference [19] where the discrete Markov chain was computed using auto-regressive models and K-means clustering to group the discrete scenario nodes. Their approach enabled the serial correlation and cross correlation between each stochastic variable to be considered.

The overall coupling between the discrete decision stages and scenario nodes are showcased in Fig. 1 on the lower part of the illustration. Each of the scenario nodes in the figure are realized values for the stochastic variables in the decomposed scenario tree. The transition probability $\rho(g, s_g|s_{g-1})$ of transitioning from scenario node s_{g-1} to s_g within N_g^S during stage $g-1$ to g is based on the probability function value between the two scenarios. This probability can be scenario-dependent, to capture how a given scenario influences the probability of future scenarios.

The uncertainty parameters within each decomposed problem are denoted as stochastic variables, which are the uncertainties in the original problem. For a specific decision stage, there exist multiple discrete scenarios which are unknown to the decomposed optimization problem.

The stochastic variables thus describe the parameters that are influenced by scenarios, and when realized for a scenario $s_g \in N_g^S$, would be given as parameters for that problem. The following stochastic variables are considered in this formulation: outdoor temperature (T_t^{out}), solar irradiation (I_t^{Irr}), electricity price (C_t^{spot}), consumer-specific electrical (D_t^{el}) and thermal load (D_t^{WT}), and EV availability (δ_t^{EV}).

2.1.2. Multi-period price signals

The two state variables used in this work have different periods in which their price signals are in effect. With the SDP framework, the EFCCs are capturing the future cost change of adjusting the state variables. It is important that the EFCCs only portrays the future cost and the influence current decision making can contribute on for the period in which the current price signals are active. The STES state variable consider the rest of the year, while the MPGT state variable only consider a month at the time. When a decision stage g transitions into a new month, the EFCC should be updated to directly capture the new monthly MPGT cost, and remove information on the old MPGT cost. The longer price signal, STES, should still contain information on the future. However, the dependencies between the two state variables must still be captured. Fig. 1 showcases the scenario coupling on stage transition, and an overview of how the multi-period price signals should be represented during the overall operational period.

As seen in the top part of Fig. 1, each stage considers two different price signals at all time.

- Signal 1, which considers the STES unit, is active for the whole year and all periods.
- Signal 2, in this case being the MPGT, have multiple activation periods.

The state variable for signal 2 during period 2 should only consider the distinct direct future cost in the EFCC, and not account for the other periods of that signal. However, since two price signals are analyzed simultaneously, their influence on each other must be accounted for and included in a period transition. Signal 1 has an influence on signal 2 for all periods, and this should be reflected in the EFCCs in each period. The marginal cost change for signal 2 would be a new price signal, and signal 1 considers the future marginal cost for itself, but also has some information on its influence on signal 2 for future periods. This extension to the SDP framework is presented in Section 2.1.4.

2.1.3. Solution strategy for SDP algorithm

The calculation of the EFCC is done through the SDP algorithm solution strategy shown in Algorithm 1. This algorithm uses the decomposed optimization problem presented in Section 2.2 to generate the EFCCs for every stage of the overall problem. More detailed explanation of the SDP algorithm is presented in [23]. The backwards procedure of the SDP framework is initiated in line 1, starting at the last decision stage and going backwards to the first decision stage. In line 2, a for-loop for every combination of initial state variable values is initiated, setting the initial condition for both state variables in line 3 and 4. In line 5, the for-loop for every scenario is initiated, and the stochastic variables are realized in line 6, given as parameter for the specific decomposed optimization problem. In line 7, the EFCC for the future decision stage $g+1$ is given as input to the specific problem, where all discrete values are set. The optimization problem defined in Section 2.2 for the specific stage g, scenario s_g and initial value n is executed at line 8, where the objective function is given as output. After, the discrete EFCC value for initial condition n, for each scenario, is calculated in lines 9-10, with weighted value from the scenario probabilities. Thus, the EFCC includes the weighted probability of future cost, based on the scenario probabilities and on what scenario we are currently in. This procedure is done for all states, until the whole EFCC has been calculated, in which the process is continues for all decision stages until we have arrived at the start of the period.

Algorithm 1: The SDP algorithm

1 **for** $g = |\mathcal{G}|, |\mathcal{G}|-1, .., 1$ **do**
2 **for** $n \in N^P$ **do**
3 $P_0^{imp} \leftarrow P_{n[0]}^{imp}$
4 $E_0^{STS} \leftarrow P_{n[1]}^{STS}$
5 **for** $s_g \in N_g^S$ **do**
6 $\{C_t^{spot}, D_t^{El}, D_t^{WT}, \delta_t^{EV}, I_t^{Irr}, T_t^{out}\} \leftarrow \Gamma(g, s_g)$
7 $C_i^{Future} \leftarrow \Phi(i, s_g, g+1)$ for $i \in N^P$
8 $C_{s_g,n} \leftarrow Optimize(1)-(11)$
9 **for** $s_{g-1} \in N_{g-1}^S$ **do**
10 $\Phi(n, s_{g-1}, g) = \sum_{s_g=1}^{N_g^S} C_{s_g,n} \cdot \rho(g, s_g | s_{g-1})$
11 **if** $g \in S_{MPGT}$ **then**
12 $\Phi(...) \leftarrow UpdateEFCC(g, \Phi(...))$

The mentioned extension to this SDP algorithm, based on multiple recurring price signals, occurs in line 11 and 12. Line 11 checks if the current stage g is within set S_{MPGT}, which contains information on the stages that experience a change in long-term price signals. In other words, it tells the timing of when a given price signal period has ended, and a new period has started. For this case, it would be for all stages where the MPGT would transition from one month to another. If g is within, this stage is the last to experience the current long-term price signal. The next stage will be exposed to a new long-term price signal, and therefore appropriate information on the future must be presented. This triggers the UpdateEFCC algorithm presented in Section 2.1.4, which will adjust the EFCC to account for the change in price signal.

2.1.4. Solution strategy for multi-period price signals

The following section details an overview over an extension to the SDP algorithm presented in Algorithm 1, which aims at adjusting the generated EFCC to remove and update recurring price signals during a longer period. The extension, which is showcased in Algorithm 2, comes into effect for stages that initiates a new long-term price signal during the overall period. Note that this specific representation only considers the MPGT to be a price signal with multiple periods, but it could be generalized to also include other price signals. This algorithm takes in information on the current decision stage g where the price signal is updated, and the current EFCC Φ for this decision stage. The overall goal of the algorithm is to adjust the marginal change in cost within the EFCC, to be reflected upon the marginal cost for the new price signal, and for the other price signal in effect.

Algorithm 2: Function UpdateEFCC(...)

1 **Input:** $g, \Phi(...)$
2 $C_{init}^{val} \leftarrow C_{init}^{MPGT}(g)$
3 $n_{init} \leftarrow P_{init}^{MPGT}(g)$
4 **for** $s_{g-1} \in N_{g-1}^S$ **do**
5 $\phi(0,0) \leftarrow \Phi(0,0,s_{g-1},g)$
6 **for** $n_0 \in N_0^P$ **do**
7 $\phi(n_0,0) \leftarrow \phi(n_0-1,0)) + (P_{n_0}^{imp} - P_{n_0-1}^{imp}) \cdot C_{init}^{val}$
8 **for** $n_1 \in N_1^P \backslash n_1 \neq 0$ **do**
9 $\phi(n_0,n_1) \leftarrow$
 $\phi(n_0,n_1-1) + \Phi(n_{init},n_1,s_{g-1},g) - \Phi(n_{init},n_1-1,s_{g-1},g)$
10 $\Phi_{new}(n_0,n_1,s_{g-1},g) \leftarrow \phi(n_0,n_1) \; \forall n_0,n_1 \in N_0^P, N_1^P$
11 **Output:** $\Phi_{new}(...)$

In line 2 of Algorithm 2, we define the new marginal cost for the MPGT that is valid for this period. This enables variation in the MPGT cost for each month. Line 3 sets the initial value for the state variable in the price-signal now ending. The for-loop in line 4 loops for every

scenario that exist for the coming decision stage $g-1$, meaning that we update every scenario-dependent EFCC. In line 5, the value from the EFCC in the (0,0) position is used as the initial value for the matrix ϕ, which will contain the new updated EFCC at the end. This initial value is used to further capture the marginal cost change with change in state variable values.

Line 6 starts a for-loop for all discrete points of the state variable with a new price-signal, n_0. The marginal cost change for the state variable is recalculated in line 7, based on the marginal cost for the new price signal C^{val}_{init}. This recalculation is only done for the dimensional direction that applies for the current state variable. This marginal cost change does not consider any information from the original EFCC, only the new cost due to the new price signal being in effect. Thus, all previous values on the marginal change in cost of operation for the MPGT is ignored.

Lines 8-9 calculate the future cost change in the dimension for the other state variable that does not have a change in price signal, n_1. Here, the future cost is portrayed as the cost for the previous discrete point n_1-1 in ϕ, plus the change in marginal cost from the EFCC, Φ, for discrete points n_1 and n_1-1. Thus, the cost change in ϕ is based on the values obtained from the EFCC. Note, that the discretized point for the state variable n_0 from the EFCC is set by the n_{init} variable determined in line 3. The use of n_{init} is important; we only want the future cost of the long-term price signal that is not updated, to be based on the initial value we will expect to encounter in the future stage. We know what initial value we would have on the price signal that would start on stage g, regardless of what we do up to this point. Therefore, we want the information on the long-term price signal still ongoing, to only contain information given that premise; we would start stage g with initial value n_{init}. For the MPGT cost, n_{init} would be 0, as you start a new month with a clean slate on peak import.

The principle of n_{init} could be applied to an uncertain initial state variable value, giving this approach more option for extensions. This value could be a list of potential values, each with a corresponding probability to occur in the future. For instance, should the price signal be on an EV that would be lent, one could assume that there are probabilities that the EV could be returned on the specific decision stage with different SoC. In that regard, the calculation done in lines 8-9 should use the weighted future cost for all possible future initial values. This point of view is left out of scope for this work.

With the setup detailed in Algorithm 2, the formulation in lines 6-9 will include the new long-term price signal C_{init}, and keep the future impact of the still ongoing price signal. Finally, line 10 stores the new EFCC. This procedure is repeated for all scenarios until returning with the new EFCCs Φ_{new}, which is given back to the original SDP framework in Algorithm 1. The resulting framework in Algorithm 2 provides a way to update the EFCCs given that there is a transition of price signals that are valid during operation, while still keeping information on other price signals that are valid. The update does not provide any direct coupling with the new price signal and the still-ongoing price signal, since there is no experience with their influence yet. However, the latter still contains marginal cost change that is influenced by the future price signals, that the SDP framework has explored but in operational terms will be activated in the future. Thus, the information in the now updated EFCC can help use the current price signal to create an efficient operational strategy, that will influence the future price signal in an overall more global fashion.

2.2. Decomposed decision problem

The decomposed decision problem is formulated as an optimization model for operating the energy system within a building or household, which could be through a home energy management system. The different flexible assets are controllable, giving flexibility on electricity usage in the building. The presented optimization model operates for a single

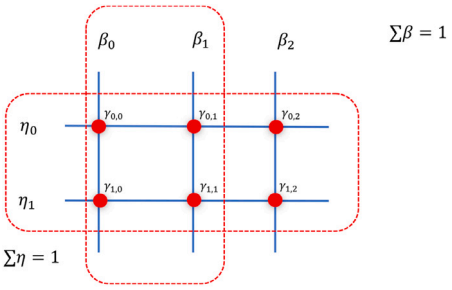

(a) Example of the two-dimensional piecewise-linear planes that ties the state variables to the EFCC. The dashing red lines show how a plane can be represented.

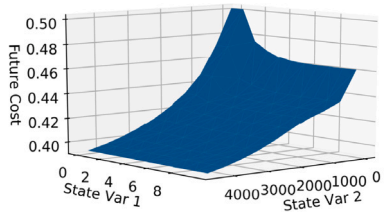

(b) Example of EFCC in 3D, which is based on both state variable values.

Fig. 2. Illustrations of how to represented the EFCC with multiple state variables.

deterministic stage of the overall SDP framework, for a given decision stage g, scenario s_g, and initial state variable values P^{imp}_0 and E^{STES}_0.

The building featured here have several flexible assets that can be controlled by the home energy management system: a Battery Energy Storage System (BESS), an Electric Vehicle (EV) charger, an air-to-water heat pump (HP), and indoor space heating. To make the transition between the decomposed decision stages feasible, each flexible asset except the STES has identical start/end values on their SoC and energy levels. This means the flexibility for these assets are limited to within each decision stage, which is due to the assets not being represented within the EFCC. In addition, there are non-flexible, non-shiftable loads that must be met at all times: electric-specific demand, and heat demand for the water tank.

2.2.1. Objective function

The objective function for the optimization problem is to minimize the total electricity cost for the end-user. The problem considers both the current cost of operation, and the expected future cost α^{future}, which is tied to the two state variables.

$$min\{\sum_{t\in\mathcal{T}}[C^{spot}_t\cdot(y^{imp}_t-y^{exp}_t)+C^{grid}\cdot y^{imp}_t]+\alpha^{future}\} \quad (1)$$

2.2.2. Expected future cost curve

The EFCC represents the future value of operation for the state variables they depend on. Based on the layout presented in [18], the piece-wise linear planes represent the future value based on two different state variables. The plane is shown as a 3D cost curve, based on the discretized states of both state variables. The illustrations of this implementation is showcased in Fig. 2. It is assumed that the problem is convex with this formulation.

Fig. 2b shows how the EFCC is illustrated, made up of multiple piece-wise linear planes. The mathematical representation is described in Eqs. (2a)-(2h), that supports the representation showcased in Fig. 2a. The discrete points of the EFCC are based on the weighting variable $\gamma_{n,m}$. The sum of all weighting variables must be equal to 1 as stated in Eq. (2a). These weighting variables are connected to the state variables β_n and η_m, as presented in Eqs. (2b) and (2c), and shown in Fig. 2a. The set $L_{x,SV}$ comprise of the indices for the weighting variables that are connected to the corresponding discrete state variable point x, for

state variable SV, which is equivalent to a corresponding row/column in Fig. 2a. Based on the discrete values for the state variables, defined in Eqs. (2d)-(2e), the variables β_n and η_m are weighted and must be equal to 1, which further on puts weights on $\gamma_{n,m}$. Then, the optimal expected future cost is found by summing all discrete cost points in the curve, based on the weighting variable $\gamma_{n,m}$ in Eq. (2f). From this formulation, the future value of the state variables are directly represented in the problem.

$$\sum_{n,m\in\mathcal{N}_P} \gamma_{n,m} = 1 \tag{2a}$$

$$\beta_n = \sum_{n_1,m_1\in L_{n,MPGT}} \gamma_{n_1,m_1}, \quad \forall n \in N_0^P \tag{2b}$$

$$\eta_m = \sum_{n_1,m_1\in L_{m,STES}} \gamma_{n_1,m_1}, \quad \forall m \in N_1^P \tag{2c}$$

$$p^{imp} = \sum_{n\in N_0^P} \beta_n \cdot P_n^{imp} \tag{2d}$$

$$E_{\mathcal{T}}^{STES} = \sum_{m\in N_1^P} \eta_m \cdot P_m^{STES} \tag{2e}$$

$$\alpha^{future} = \sum_{n,m\in N^P} \gamma_{n,m} \cdot C_{n,m}^{Future} \tag{2f}$$

$$\gamma_{n,m} \geq 0 \quad \forall n,m \in N^P \tag{2g}$$

$$\beta_n, \eta_m \geq 0 \quad \forall n,m \in N^P \tag{2h}$$

2.2.3. Electrical energy balance

The electric energy balance in the building is given in Eq. (3). The energy balance covers import and export of electricity to the grid, charge and discharge from the BESS, load from EV and HP, and the non-elastic electrical demand.

$$y_t^{imp} - y_t^{exp} + y_t^{B,dch} + y_t^{PV} = D_t^{El} + y_t^{EV,ch} + y_t^{HP} + y_t^{B,ch} \quad \forall t \tag{3}$$

2.2.4. Measured peak grid tariff

The constraints regarding the MPGT is showcased in Eqs. (4a) and (4b). The variable p^{imp} sets the highest single-hour peak import during the operational period, which is limited by either the historical initial peak import P_0^{imp}, or by the hourly import quantity y_t^{imp}. The constraint is connected to the EFCC through Eq. (2d).

$$p^{imp} \geq P_0^{imp} \tag{4a}$$

$$p^{imp} \geq y_t^{imp} \quad \forall t \tag{4b}$$

2.2.5. Electric vehicle

The behaviour of the EV is formulated in (5a) to (5c). The EV is modelled as a uni-directional battery that can be charged at a continuous rate when available. The availability, set by the stochastic variable δ_t^{EV}, determines if the EV is chargeable, or discharged with a constant load when not available. The EV must stay within a time-depending specific range in its SoC in (5c).

$$E_t^{EV} - E_{t-1}^{EV} = y_t^{EV,ch}\eta_{ch}^{EV}\delta_t^{EV} - D^{EV}(1-\delta_t^{EV}) \quad \forall t \tag{5a}$$

$$0 \leq y_t^{EV,ch} \leq \dot{E}^{Max} \quad \forall t \tag{5b}$$

$$E_t^{EV,min} \leq E_t^{EV} \leq E_t^{EV,max} \quad \forall t \tag{5c}$$

2.2.6. Battery energy storage system

A bi-directional BESS is available within the building with the characteristics shown in (6a) to (6d). The battery can be discharged and charged at a continuous rate, with limitations on power capacity and a storage capacity range.

$$E_t^B - E_{t-1}^B = y_t^{B,ch}\eta_{ch}^B - \frac{y_t^{B,dch}}{\eta_{dch}^B} \quad \forall t \tag{6a}$$

$$0 \leq y_t^{B,ch}\eta_{ch}^B \leq \dot{E}^{B,ch} \quad \forall t \in \mathcal{T} \tag{6b}$$

$$0 \leq y_t^{B,dch} \leq \dot{E}^{B,dch} \quad \forall t \in \mathcal{T} \tag{6c}$$

$$E^{B,min} \leq E_t^B \leq E^{B,max} \quad \forall t \tag{6d}$$

2.2.7. Photovoltaic system

A roof-mounted PV system is connected to the electrical system through a controllable system. The home energy management system is assumed to be able to adjust the power output up to maximum time-dependent production.

$$0 \leq y_t^{PV} \leq A^{PV} \cdot \eta^{PV} \cdot I_t^{Irr} \quad \forall t \in \mathcal{T} \tag{7}$$

2.2.8. Thermal system

The thermal system is made up of the following appliances: An air-to-water HP that supplies heat, an STES that can store and deliver thermal energy, a non-flexible non-shiftable water tank with thermal demand, and an outlet to supply the indoor space with heat.

The HP is generating heat based on the electrical input with a constant Coefficient Of Performance (COP) factor to convert electrical energy to thermal energy. The COP of a HP is normally not treated as a constant and is influenced by the temperature deviation between the heat source temperature (outdoor temperature for air-sourced HPs) and the temperature of the STES [11]. Our simplification with a constant COP means the HP does not capture higher performance during summer with low temperature deviation and does not capture lower performance during winter with colder outdoor temperature. Thus, this constant COP could shift to more favourable use of HP during the winter than if this was captured accurately, which would also decrease the need for the STES. It is assumed the HP can be operated continuously up to the rated electrical capacity.

$$y_t^{HP,out} = COP^{HP} \cdot y_t^{HP}, \forall t \tag{8a}$$

$$0 \leq y_t^{HP} \leq P^{HP}, \forall t \tag{8b}$$

The thermal energy balance is shown in (9). Thermal energy is supplied from the HP and/or the STES, to cover demand from space heating, the water tank, or excess thermal energy stored in the STES. The water tank is seen as a time-dependent load parameter.

$$y_t^{HP,out} + y_t^{STES,out} = D_t^{WT} + q_t^{sh} + y_t^{STES,in} \quad \forall t \tag{9}$$

The STES consist of a storage tank with a rated storage capacity. The storage unit can store or deliver thermal energy up to a rated capacity in both directions. The STES is formulated as a big thermal energy tank, with only losses associated with a fixed efficiency loss parameter, effective at the first hour of operation in Eq. (10a), to simulate losses. The energy balance for each time step is given in Eq. (10b). The inflow and outflow restriction of thermal energy in Eqs. (10d)-(10e) are time-dependent and part of the stochastic variables, making it possible to set this as seasonal limitations. This option enables the flow of thermal energy to be limited not only on capacity, but also on availability for storing/delivering heat.

$$E_t^{STES} - E_0^{STES} \cdot (1-\eta^{STES}) = y_t^{STES,in} - y_t^{STES,out}, t = 1 \tag{10a}$$

$$E_t^{STES} - E_{t-1}^{STES} = y_t^{STES,in} - y_t^{STES,out}, \forall t \tag{10b}$$

$$0 \leq E_t^{STES} \leq E_{Rated}^{STES}, \forall t \tag{10c}$$

$$0 \leq y_t^{STES,in} \leq \dot{E}_t^{STES,in}, \forall t \tag{10d}$$

$$0 \leq y_t^{STES,out} \leq \dot{E}_t^{STES,out}, \forall t \tag{10e}$$

The indoor space heating system is modelled in this work to be able to capture the dynamics of heating demand. The space heating system is presented as a grey-box model and formulated as a linear state-space model in continuous time [24,25]. This work, as is explained and performed in [25], represents the space heating system as an RC-network model on an hourly resolution, whereas this optimization problem represents the system by formulating a two-resistance two-capacitance (2R2C) RC-network model in Eqs. (11a)-(11d). The 2R2C model represents the thermal responses of the building as capacitances and resistances, that all influence the need for providing heat to cover space heating demand. The capacitances describe the thermal response of the light and heavy building envelope elements. The resistors describe the heat transfer between the indoor environment, building elements, and the outdoor environment. The thermal energy provided by the thermal system heats the indoor area and can be heated continuously up to the rated capacity. The indoor area has a flexible temperature boundary within comfort levels for the users. The dynamics of space heating can be represented in finer detail, as presented in [25,26], but for this work is kept as a 2R2C RC-network grey-box model.

$$0 \leq q_t^{sh} \leq \dot{Q}^{sh} \quad \forall t \tag{11a}$$

$$T_t^{in,min} \leq T_t^{in} \leq T_t^{in,max} \quad \forall t \tag{11b}$$

$$T_t^{in} - T_{t-1}^{in} = \frac{1}{R_{ie}C_i}[T_{t-1}^{e} - T_{t-1}^{in}] + \frac{1}{C_i}q_t^{sh} \quad \forall t \tag{11c}$$

$$T_t^{e} - T_{t-1}^{e} = \frac{1}{R_{ie}C_e}[T_{t-1}^{in} - T_{t-1}^{e}] + \frac{1}{R_{eo}C_i}(T_{t-1}^{out} - T_{t-1}^{e}) \quad \forall t \tag{11d}$$

Note that the representation of the indoor space heating system as a linear state-space model is a simplified representation compared to advanced building simulation methodology, for example including spatial variability in temperatures, surface-specific characteristics, and more detailed representation of inertia and thermal mass distribution. However, such simplifications are common in optimization models focusing on techno-economic optimization towards economic objectives [27,28], and we therefore deem the simplified representation of thermodynamics sufficient for the purpose of this paper.

3. Case study

The presented model is applied on a case study surrounding a realistic Norwegian building in southern Norway. The building, denoted as a single-family house, uses a home energy management system to control the different flexible assets and keep track of the energy usage in the building. The data is for the year 2019, with hourly time resolution per day. The stochastic variables used in this study consist of both historical and synthetic data.

3.1. Building structure

The building has an electric-specific consumption profile that covers the residents inelastic electricity usage. The inelastic electricity usage is based on data from the Distributional Operator Ringerikskraft from 2017 [29].

3.1.1. Electric vehicle

An EV with a 24 kWh battery is selected for this study, with an SoC range between 20-90%. The EV charger is rated at 3.7 kW with 85% efficiency, and can be operated continuously. During departure, the EV is required to have an SoC range between 60-90%. Based on [30], a mean driving distance of 52 km has been used. Assuming a consumption rate of 18 kWh/100 km, the hourly discharge rate is at 1.02 kWh/h for D^{EV} with a 9-hour offline timeframe. The offline timeframe is set between 9 AM to 5 PM for weekdays and weekends based on observations in [30].

3.1.2. Battery energy storage system

The BESS installed in this system is based on a battery from Sonnen-Batterie [31]. The rated power input/output is set at 2.5 kW measured at the output of the inverter, with an installed capacity of 5 kWh. The BESS can be operated between 10-100% SoC, with a round-trip efficiency of 85% [32]. Degradation effects are left out of this analysis.

3.1.3. Thermal structure and seasonal thermal energy storage

The space heating dynamics is based on observed values from the Living Lab building built by Zero Emission Building (FME ZEB)[1] and NTNU [33,34]. The default temperature boundary for space heating is between 20-24 $°C$, which from reference [35] is the range end-users find comfortable. The DHW-consumption profile is based on measurement of 49 water heaters at Norwegian households through the "Electric Demand Knowledge - ElDek"[2] research project by SINTEF Energy Research [36]. The data here is given as electric demand, which we consider inflexible and with a 1:1 electric to heat conversion rate.

The heat production is based on a small-scaled air-to-water HP with a rated electric capacity of 3 kW, and a constant COP at 1.5 over the year. The HP is connected so it can deliver heat to the thermal system, which can provide thermal energy to the STES, space heating and domestic hot water directly. The STES is represented as a large-scale storage unit. For simplicity of this study, the STES is portrayed as a storage unit without any dynamic dependencies on the surrounding, similar to the STES in [16]. To account for losses, the STES has a constant efficiency loss at the start of each operating day set at 0.16%, which amounts to about 60% losses over the course of a year. The STES, here assumed to be a water tank, has a rated capacity at 5000 kWh, with heat flow in/out rated at 5 kW. As thermal systems have high inertia, we allow the STES only to be charged during the summer period (May-Oct), and only discharged during the winter period (Nov-Apr), but with continuous rating.

Existing literature has found COP-values for HPs used with STES to be around 4 [11], but this is very dependent on the STES solution and medium. Our work has chosen a lower constant COP for the HP at 1.5, due to the simple description of the STES, and to add some padding on the seasonal variation surrounding the COP.

3.1.4. Initial conditions flexible assets

The flexible assets not part of the EFCC have the following start/end values during stage transition: $T_0^{in} = 22\,°C$, $T_0^{e} = 20\,°C$, $E_0^{EV} = 14.4$ kWh, $E_0^{B} = 2.5$ kWh. This limits their flexibility to only contribute towards in-day variation, which is due to decomposing the overall problem.

3.1.5. Grid tariff structure

The MPGT structure is based on the grid tariff prices from 2019, by Agder Energi Nett [4]. This MPGT is currently limited to consumers with yearly consumption above 100 MWh/year, but we assume for this analysis to be a valid option for all consumers regardless of demand profile. An alternative version of this MPGT has been introduced for smaller end-users from summer 2022. For this one, the average of the three highest day-based hourly peak imports are considered for setting the peak-consumption, but this is not accounted for in this study [37]. The monthly MPGT has seasonal prices depending on the summer and winter periods, set at 4.458 $\frac{EUR}{kW \cdot month}$[3] during the summer period (May-Oct), and 13.375 $\frac{EUR}{kW \cdot month}$ during the winter period (Nov-Apr) [4]. In addition, the grid tariff contains a volumetric cost at $0.02616 \frac{EUR}{kWh}$, which covers both the DSOs volumetric charge and the fixed consumer cost from the government. Also, a monthly fixed cost of 6.25 EUR is included in the overall cost. All numbers here include a value added tax

[1] www.fmezen.no/.

[2] https://www.sintef.no/prosjekter/eldek-electricity-demand-knowledge/.

[3] Assuming a 10 NOK/EUR conversion rate.

at 25%. The electricity spot price data is based on bidding zone NO2 in Norway, from Nordpool for the year 2019 [38].

3.2. Scenario generation

The SDP algorithm allows uncertainty to be included in the operational strategy, which reflects the operational decision by the home energy management system. To limit the range of uncertainty, the case study only considers uncertainty within the outdoor temperature. Information such as electricity price and electric-specific demand is considered deterministic.

In total, three scenarios per day have been generated. The three scenarios are based on a normal distribution of the weather effects, with the mean and standard deviation as the discrete scenarios. Data for the weather effects have been obtained from Renewables.ninja [39], for the period of 1980-2019 using the MERRA-2 tool [40] with a population-weighted factor for Norway. The historical data were used to create hourly normal distributions on the outdoor temperature, to generate three discrete scenarios per day, consisting of the mean and the standard deviation in both directions. The probability distribution for the future scenario nodes is identical regardless of the current operating scenario.

3.3. Model cases

This work aims to showcase the strategy framework for a residential building with an STES and a monthly MPGT cost over the course of one operational year. The STES is able to reduce the total cost by storing thermal energy during summer and deliver during winter to cover the thermal demand. This asset contributes to lowering the MPGT cost during the winter period, and storing thermal energy long-term.

It is important to analyze and investigate how the SDP framework performs with the addition of recurring MPGT costs, and with the inclusion of a seasonal storage unit. The analysis should investigate the strategic planning for both price signals, individually and coupled together, to gather an overview over their influence on each other. This includes how the EFCC are generated and their strategic behaviour, but also the economical performance over an operating year. Only import of electricity is deemed as the electrical source for creating and storing thermal energy in the STES, making both price signals coupled to each other. This analysis will investigate the following cases regarding STES and MPGT:

- Case 1: Only MPGT
- Case 2: Only STES
- Case 3: Both MPGT and STES

Case 2 will still include the MPGT cost in the economic analysis with a peak import limit of 10 kWh/h, but the MPGT-impact is not being part of the EFCCs. Therefore, Case 2 will operate on the basis of dismissing the MPGT price signal.

For all the three cases we analyze in this work, they will be solved for three separate instances. Case X (SDP) considers the SDP framework, exploring the accuracy and performance of the presented methodology. Additionally, a yearly optimization problem of the exact same energy system with Perfect Information (PI) on the uncertain parameters will be performed, to compare how much influence uncertainty has on operation. These PI-instances provide the best solution that is acquirable for the given problem and does not make use of the EFCCs for MPGT and STES, as the whole year of operation is considered. The comparison of the PI-instances and the SDP framework provides information on the expected value of perfect information, which tells how much additional improvements can be performed if uncertainty was eliminated. For each case, two PI-instances exist: Case X (PI 24) limits the problem to keep the same initial conditions for the flexible assets for every 24 hour, upholding the restrictions caused by decomposing the problem. Case X (PI) does not include this constraint, allowing flexibility between days from these assets.

For the SDP-instances, the case analyzes an operational year with 365 daily decision stages and 3 scenarios per stage. As the STES is expected to be empty at the start of the summer period, the operation starts on May 1st and ends on April 30th. The peak import state variable for MPGT has 51 discrete points between 0-5 $\frac{kWh}{h}$, while the SoC for the STES has 201 discrete points between 0-5000 kWh, amounting to 30 753 states per stage, a total of 11.22 million instances to analyze for the whole year. The SDP framework has been coupled to multiprocessing, as each state within decision stages can be solved independently of each other. The problem was developed and solved with Python and the optimization package Pyomo [41], using two AMD EPYC 7H12 64-core processors. For case 3 with MPGT and STES, the run time is about 25 hours.

The performance of the SDP framework and the created EFCCs is investigated through a simulation phase. The yearly performance is analyzed by a day-by-day operation over the year with the EFCCs as input to represent the future influence of operation. We operate starting at May 1st (denoted as day 0), and sequentially solve a decomposed decision stage with the EFCC as input, and use the resulting state variable values as input for the next decision stage, until arriving at April 30th. For each day, a discrete scenario is drawn, based on the probability. The yearly analysis is performed 1000 times with different scenario combinations, to analyze the overall performance and to capture the role of uncertainty. These scenario combinations and number of simulations are the same as the PI-instances consider.

4. Results & discussion

This section presents the results from the case study, focusing on the operational strategy and the economic performance of the analysed building. Section 4.1 presents the EFCCs generated for specific stages during the operational year for cases 1-3 (SDP) as an output from the SDP framework. This analysis will examine the strategic behaviour of the EFCCs for each price signal, to capture any specific trends and correlation between them. Further on, Section 4.2 will present the economic performance of each SDP-instance, where the EFCCs are used in a performance simulation. Both the economic performance over the year and the operational performance of the STES and MPGT will be included, to capture any strategic trends and how these correlate to the EFCCs' behaviour. Lastly, the operational performance from the SDP methodology compared to the PI-instances will be explored in Section 4.3.

4.1. Generation of future cost curves

As presented in Section 2.1.3, the SDP framework in Algorithm 1 creates an operational strategy for the building over the entire year. The operational strategy is showcased as stage-wise EFCCs, which show the changes in future cost based on the peak import level and changes in the STES SoC. The future cost of the STES showcases the future value of changing the STES SoC, by either storing or delivering heat. The EFCC for MPGT peak import shows the added cost of increasing the maximum peak to enable increased electricity imports. The peak import denotes the MPGT cost, which, through the extension of the SDP algorithm in Algorithm 2, is only directly represented in the EFCC for each respective month that it is active. This enables the EFCCs to consider the monthly cost influences, and the yearly strategy for the STES SoC. For different months, the strategy changes for both the MPGT and STES, based on the cost of capacity, and the need for thermal energy (seasonal variation). To capture the variation of strategic behaviour during summer and winter, each case will present the EFCCs for two distinct days over the year. The optimization model starts at May 1st, which is denoted as day 0 of the analysis period. The following days will be emphasized to showcase

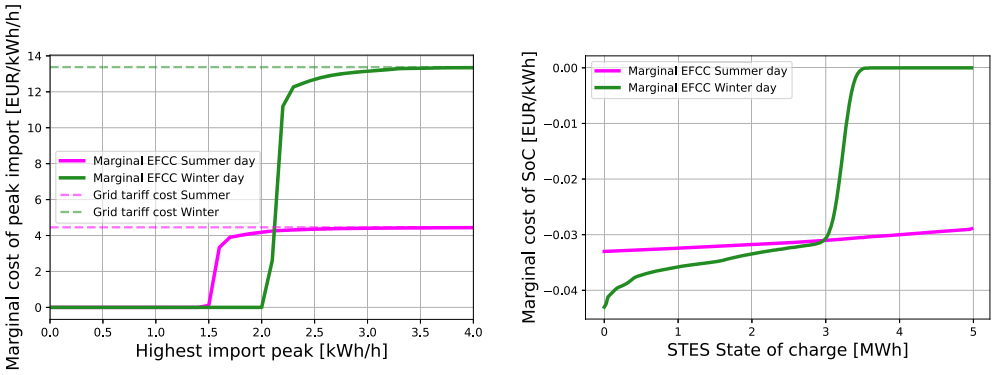

(a) Plot of the marginal EFCC for only the MPGT in Case 1, for both the summer and winter day.

(b) Plot of the marginal EFCC for only the SoC of the STES in Case 2, for both the summer and winter day.

Fig. 3. Plots of the marginal EFCCs for Case 1 and Case 2.

the EFCCs: a summer day, which considers September 19th, and a winter day, which looks at February 6th. The EFCCs are only created for the SDP-instances, and as such, we will only refer to these instances in this subsection.

The decision strategy is influenced by the marginal cost change within the EFCCs. As such, every visualisation of the future cost curves will be showcased as marginal EFCCs, where only the marginal change is captured for increasing state variable values. This also enables the marginal EFCCs to be compared between different stages, as the total future cost is ignored in favour of the marginal change.

In the following subchapter, a short description of the main observations regarding the EFCCs in Case 1 and Case 2 will be given. More detail and explanation regarding these two cases can be found in Appendix A.

4.1.1. Case 1 - only measured peak grid tariff

The cost curves generated in Case 1 only account for peak import costs within the SDP framework. The EFCCs describe the increase in the cost of operation for each month when increasing the highest single-hour import of electricity. The marginal EFCC for Case 1 is shown in Fig. 3a, which includes both summer and winter days. Increasing peak import increases the marginal future cost, due to having the higher monthly MPGT cost. The marginal future cost does not correlate directly with the MPGT cost, since increasing peak import results in increased benefits during operation, with load shifting to account for spot-price variation. However, beyond a certain limit, the increased peak import produces no additional benefits. The strategic peak import in Fig. 3a changes for summer and winter days. The most distinct difference between the two days is the initial value of peak import, where the marginal cost is non-zero. For the summer day, the non-zero value initiates around 1.5 kWh/h, and around 2.0 kWh/h for the winter day, which is due to the high thermal demand during winter. The MPGT cost is three times less in the summer month than the winter month, making peak-shaving during winter more cost-effective than during summer. Therefore, the seasonal variation in MPGT cost promotes peak shifting between the seasons.

4.1.2. Case 2 - only seasonal storage

Case 2 generates cost curves that capture the future value of altering the STES SoC during operation. Since the only source of thermal energy is electricity, spot-price variation between summer and winter acts as motivation for long-term energy storage. The marginal EFCC for Case 2 is depicted in Fig. 3b, which includes both a summer and winter day. The marginal cost is negative, as an increase in SoC decreases the future need to import electricity. For the winter period, which can only discharge, the marginal value depends on whether the cost-optimal strategy is to discharge the thermal load now, or store it for future use. For the summer period, which can only charge the STES, the marginal value depends on whether the marginal unit could be stored in a future summer month at a more cost-optimal price, but also the cost that this marginal unit would replace during the winter period. As such, the cost curves for both periods show different strategies for using the STES, to make use of seasonal storage capabilities in a cost-optimal manner.

4.1.3. Case 3 - both price signals

Case 3 includes both the STES and MPGT price signals as part of the SDP framework. This leads to the EFCCs having two different directions in terms of marginal cost change, one for each of the state variables. Additionally, the dimensions of each marginal EFCC are also increased by one, as they still capture the change in cost for each state variable. Therefore, each EFCC results in two distinct marginal EFCCs, which will be presented here.

Measured peak grid tariff

When only considering the operational strategy for the MPGT, the goal is to find the cost-optimal peak import level over each month. The seasonal influence that the STES gained by storing thermal energy from summer to winter should influence the peak import and MPGT cost by shifting the peak consumption from winter to summer. The marginal EFCCs for both the summer and winter day are showcased in the upper half in Fig. 4 for the MPGT state variable. In general, the Y-axis of these heatmaps showcase the state variable value for the MPGT, while the X-axis depicts the SoC for the STES. The colour change corresponds to the marginal cost change for increasing peak import.

Both figures showcase the same trend previously shown in Case 1 regarding the MPGT; low initial peaks have 0 value due to being not feasible or economically optimal, and high peaks have a value approaching the marginal cost for the grid tariff in the corresponding season. However, the main differences that can be seen here are when the marginal increase in cost starts, and the extent it is influenced by the SoC for the STES. Fig. 4a shows that for high SoC in the STES on the summer day, the marginal cost for peak-import is similar to Case 1, in terms of the transition from non-zero marginal to maximum marginal cost. However, for decreasing SoC, this boundary starts to expand, resulting in a different distribution of peak import levels to aim for, and the marginal cost increases to the grid tariff cost. For SoC around 0, the non-zero marginal cost starts at around 3.5-4 kWh/h, indicating that it is beneficial to increase the peak import level in order to increase the SoC of the STES. For increasing SoC, the highest marginal cost stays at around 4 kWh/h, but the non-zero boundary starts to expand to include lower peaks. This trend indicates that for increasing SoC, there is less need to increase the peak import. The fact that only a near-full SoC in the STES procures the same result as for Case 1 indicates that the strategy has changed with the seasonal storage, resulting in additional benefits from increasing SoC in the current period.

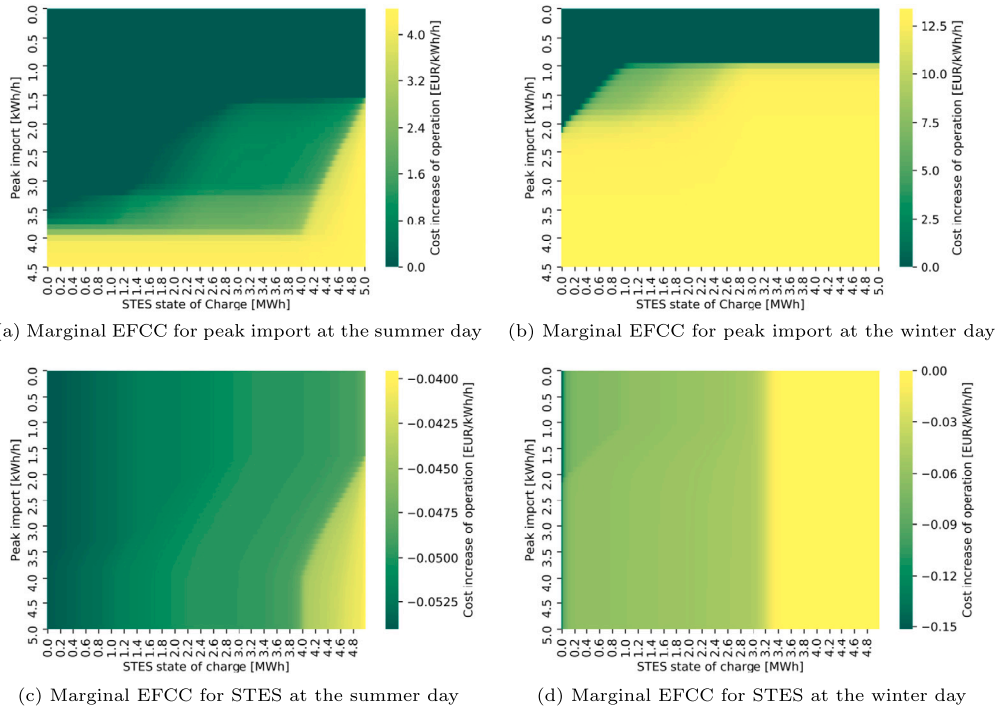

(a) Marginal EFCC for peak import at the summer day (b) Marginal EFCC for peak import at the winter day

(c) Marginal EFCC for STES at the summer day (d) Marginal EFCC for STES at the winter day

Fig. 4. Heatmap of the marginal EFCCs for peak import and STES for two specific days of the year for Case 3. (For interpretation of the colours in the figure(s), the reader is referred to the web version of this article.)

Likewise, when studying the winter day in Fig. 4b, the SoC in the STES also heavily influence the highest peak import in the strategy. Here, the strategy would be to use stored thermal energy to prevent increasing peak import, which would make it possible to achieve a peak import level of around 1 kWh/h. As the SoC decrease, the 0 marginal value decreases to 2 kWh/h at 0 SoC, which was also seen in Case 1. The peak import goal must also be readjusted to ensure sufficient thermal demand can be met. This strategy would balance the remaining SoC for both this month of operation and for the future months of the year. Therefore, scarce values of stored energy would promote higher peak import, to save the marginal energy for the few critical peaks in the future. And since the winter period has a higher MPGT cost, the penalty of having insufficient thermal energy is higher in winter than the summer, which supports the strategy of increasing peak import to store more thermal energy during the summer day. This demonstrates that, for both summer and winter, the strategy is to actively plan the highest peak import based on the current SoC in the STES, to ensure that the MPGT operation is cost-effective over the year.

Seasonal storage

The operational strategy for the STES is to find the optimal SoC throughout the year. The marginal value for SoC illustrates the value of storing thermal energy for the future load demand, which involves comparing the current cost with the future cost. The marginal EFCC for the STES SoC state variable is illustrated in the lower half in Fig. 4 for both a summer and winter day. As shown in both figures for the STES marginal EFCC, the future cost of increasing/decreasing stored thermal energy is based on both the current peak import level and the current SoC. With increasing SoC, the added value of more heat decreases, since the thermal energy would prioritise the costly needs first.

For the summer day in Fig. 4c, the operational strategy focuses on storing more heat cost-optimally for the upcoming winter period. Increasing SoC in general means the marginal benefit decreases, since the additional unit would cover a marginally cheaper future energy demand. The peak import influences the marginal benefit of the STES SoC, as an increasing peak import results in decreasing marginal value for the SoC. This is especially noticeable at high SoC, where the curve has a steep decrease in benefit. With a low peak import level, the need for load shifting increases, providing less opportunities to produce and store heat without influencing the peak. This low peak import would limit the opportunities for thermal energy storage in the future, which is why the EFCC showcases a higher future value of increasing SoC. For higher peaks, the future value decreases due to more import capacity in order to avoid shifting other flexible assets. The added flexibility also produces more cost-optimal opportunities to store heat and prioritise variation in spot-prices in the future.

The strategy for the STES changes when entering the winter period, where delivering heat becomes more important. The marginal EFCC for the winter day is shown in Fig. 4d, where the marginal benefit increases for decreasing SoC. The shape of the curve for a fixed peak import is the same as for Case 2, where the marginal benefit is 0 for high SoC (indicating excess thermal energy), with a drastic benefit increase for lower SoC. In Fig. 4d, when the initial peak is low and the STES is near empty, the targeted current peak import level could be threatened by a lack of thermal energy before the period has ended. This is reflected by the high marginal benefit, as the marginal unit could help avoid increases in MPGT cost. For increasing peaks, there is a slight decrease in future benefit, which means that the STES is not needed for peak-shaving, and thus the need for thermal energy in the current period is less critical. This trend is also influenced by the current month of operation and the future months.

An interesting observation for the summer day in Fig. 4c is that the curve has no similarity to the summer day in Case 2 shown in Fig. 3b in terms of values. The marginal benefit for STES SoC in Fig. 4c is much higher than for Case 2, regardless of peak import level. This shift in benefit demonstrates the added value that the STES offer in terms of peak import reduction throughout the winter month. Similar observations can be made for the winter day in Fig. 4d, which has a higher marginal benefit especially at lower SoC. The high benefit when the SoC is close to 0, indicates that this is necessary to decrease the peak import in the future, and that the little SoC should be saved for the critical situations. That the benefit is high regardless of peak import, indicates that it could be used for the scarce hours in the current month, but also benefit for

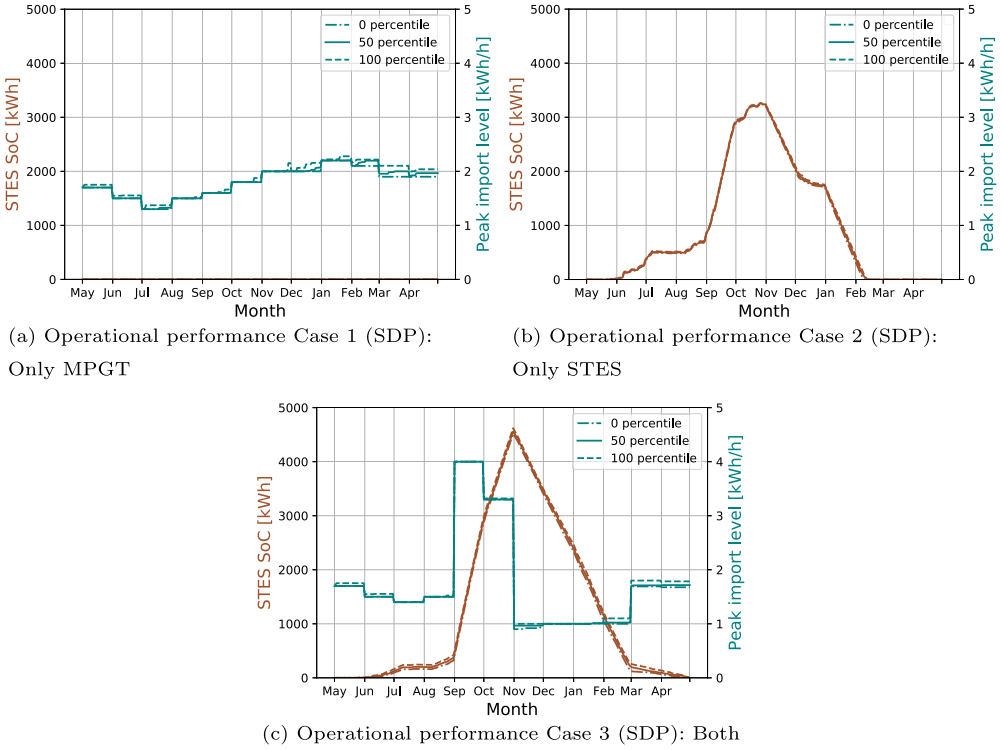

(a) Operational performance Case 1 (SDP): Only MPGT

(b) Operational performance Case 2 (SDP): Only STES

(c) Operational performance Case 3 (SDP): Both

Fig. 5. Operational performance for peak import and STES SoC over the year for all 3 SDP-instances. 0, 50, and 100 percentiles are plotted to showcase the variation in operation.

the future months. This shows that the strategic value for the STES SoC has increased, resulting in additional benefits through decreasing the peak import levels in the future, reflected by the higher marginal benefit.

4.2. Economic operational performance

The economic operational performance for the SDP-instances are analysed by computing one year sequentially, day by day. In daily problems, only information on historical peak import and STES SoC from the previous day, the stochastic variables for the specific scenario of the day, and the EFCC for the future, are given. The average economic operational performance for the three cases, for all instances, are shown in Table 1, including costs from the MPGT, import and export. For Case 2, the MPGT cost is calculated afterwards, as it does not consider the cost during operation.

4.2.1. Operational performance

The operational performance of the three SDP-instances are affected by how we strategically deal with both peak import and use of the STES during the year. As mentioned earlier, the goal is to operate cost-optimally over the whole year of operation. The cost of operation is linked to the cost of electricity to cover demand and the MPGT cost. The flexible assets available in the building manage the daily short-term flexibility potential, as they have no direct long-term cost connections due to not being part of the future cost curves. The STES have long-term flexibility potential by being able to store thermal energy from the summer to the winter, reducing the need to import electricity to cover thermal demand during winter. All of these operational performances are dependent on the price signals they are exposed to, and the technologies available. Fig. 5 visualises how the three SDP-instances perform over the year in terms of the highest peak import during each month and the yearly change in STES SoC.

Case 1 (SDP) shows how the peak import stays at around 1.5 $\frac{kWh}{h}$ during the summer period, and increases to around 2 $\frac{kWh}{h}$ during winter, showing an increased need of peak import due to increasing thermal demand from heating. Due to decomposition, which limits flexibility to daily operation through the BESS, EV and space heating, there is little flexibility to shift between days and seasons, other than the strategic knowledge of the cost for increasing peak import through the EFCC. There are some small variations in the peaks that can be seen through the percentiles, which correlates to the uncertainty in load for each day. The EFCCs offer a cost-optimal strategy given the uncertainty, which in some cases would be readjusted underway due to either higher loads or increased benefit from load shifting. The variation is most noticeable during the winter months, which correlates to the uncertainty in thermal demand.

For Case 2 (SDP) with STES, the SoC increases steadily from June towards end of October, almost for the entire summer period. September in particular is the month when the SoC increases the most: from around 500 kWh to 3000 kWh, with the maximum SoC at around 3250 kWh at the end of the summer period. Overall, the peak import level reaches 10 kWh/h each month, which was the upper limit in the optimisation problem. In the winter period, the strategy is primarily to discharge the STES during the early winter months. November and January have the highest discharge rate in the STES, resulting in the STES being empty around February. That the STES is being filled and discharged during the year, shows that it contributes some monetary value to the yearly cost of operation, and is able to cover thermal demand during winter from the energy stored during summer. The EFCC provides continuous information on the future benefit of storage in the STES, to find the cost-optimal periods for discharge.

Both the MPGT and STES are present in Case 3 (SDP), demonstrating how their operational performance is linked. The trend, compared to both Case 1 (SDP) and Case 2 (SDP), is quite obvious. First, the use of the STES has increased by increasing the charging of thermal energy during the summer, and likewise increasing its usage during winter. The charging strategy is similar to Case 2 (SDP) in that the STES is charged during the later summer months. However, the STES is further charged in October to 4500 kWh, increasing the stored energy by 50% compared to Case 2 (SDP). During winter, the STES is discharged heavily during

the first four winter months, with the little leftover SoC being used in the final winter months. The increase of months covered shows that the increased SoC is used and distributed between additional months to meet demand. Both Case 2 (SDP) and Case 3 (SDP) see little variation in the STES SoC over the winter period, despite the uncertainty. Small variations in outdoor temperature have limited influence on the operation of the seasonal storage unit. The overall goal of the STES is to store energy throughout seasons, and provide stable thermal energy during winter, whereas the uncertainty in demand is covered by the electrical side during operation.

The MPGT in Case 3 (SDP) sees a high peak import level for the two summer months when the STES is charged. September has increased the peak import level from around 1.5 $\frac{kWh}{h}$ to 4 $\frac{kWh}{h}$ when compared to Case 1 (SDP), which is uniquely to increase the STES SoC. This is also continued in October, but for a lower peak import level. For the winter period, this increased STES SoC leads to a decreased peak import level in every winter month. For the first four months, where the STES is heavily discharged, the peak import is reduced from around 2 $\frac{kWh}{h}$ to 1 $\frac{kWh}{h}$, while the last two months have some small reduction as well. It is clear that the seasonal storage is strategically used to decrease the expensive winter peak import months. The increase in peak during the summer is strategically deemed cheaper, and leads to higher cost savings throughout the overall year.

The introduction to the MPGT coupled with STES, leads to additional value in performing seasonal load shifting. While Case 2 (SDP) only focused on spot-price variation as a means of storing thermal energy, Case 3 (SDP) gives a new dimension of saving by load shifting the MPGT cost. Since charging the STES is done during the summer period, when the MPGT cost is low, the natural STES operation provides an additional benefit, which can be further increased when MPGT is considered. For the early summer months, the STES operation is similar in both Case 2 (SDP) and Case 3 (SDP), using the flexibility to partially increase the SoC, without any noticeable change in the peak import. The winter period tries in Case 2 (SDP) to reduce thermal demand in the early months, which is still prioritised in Case 3 (SDP). The one exception to the strategy is seen for December, which in Case 2 (SDP) only saw small STES discharge, but in Case 3 (SDP) saw a similar thermal energy coverage as the others. This suggests that, for this month especially, the spot price variation and value is not interesting, but the savings from the MPGT cost make it worthwhile to further increase the STES usage. Overall, this operational performance demonstrates that coupling MPGT with STES adds a new dimension of operation, as they can strategically assist each other.

4.2.2. Economic performance

The economic performance of the three cases and all instances are showcased in Table 1, alongside the PI-cases, which will be explained in detail later. Case 2 (SDP) has a very high total cost due to the MPGT cost, which is neglected during operation. The 10 kWh limit is achieved every month, making all instances in Case 2 very costly due to ignoring a vital cost component in the total cost of operation. Case 3 (SDP) sees a decrease in total operating costs compared to Case 1 (SDP) and Case 2 (SDP) by 4.6% and 69.0%, respectively. The main cost reduction compared to Case 1 (SDP) originates from the decreased grid tariff costs, but the cost also reduces somewhat due to the electricity price purchase. Case 2 (SDP) and Case 3 (SDP) have a higher electricity import than Case 1 (SDP), which comes from the use of the STES and the associated storage losses. Comparing Case 3 (SDP) to Case 1 (SDP), the main cost reduction comes through decreased MPGT cost, which has been reduced by 23.9% with the introduction to the STES. This study does not consider if these savings would cover the investment cost of an STES. Despite the increase in import of electricity to cover the losses in the STES, the electricity cost has decreased in Case 3 (SDP) by 3.4%, which stems from the spot-price variation between summer and winter. This leads to a 4.6% yearly cost reduction for Case 3 (SDP), with an STES included.

Case 2 (SDP) has an especially high operating cost due to the MPGT cost, which is not considered during operation. However, Case 2 (SDP) has the lowest electricity cost of all cases due to the use of the STES for seasonal variations in spot-prices. Despite the increase in import, the seasonal variation in spot-price makes it more worthwhile than for Case 1 (SDP) and Case 3 (SDP). The electricity cost for the year as shown here, showcase the potential for savings when using the STES when disregarding any peak import cost. The electricity cost in Case 3 (SDP) has increased by 4.3% compared to Case 2 (SDP), due to considering the MPGT cost. This operation shows a trade-off between the two costs: how to balance cost reduction of the MPGT while purchasing cheap, spot-price electricity. The use of the STES is not only to take advantage of the seasonal variations in spot-price, but also to lessen interaction with the grid. Therefore, importing electricity to increase the STES SoC during the summer has an increased cost, due to the additional winter MPGT cost-savings, and the increased import from higher losses.

Case 1 (SDP) is seen as the baseline case in terms of not having any seasonal influence on operation. The strategy framework can only showcase the value of accounting for MPGT in each corresponding month, and not have any means of impacting other months. Since the winter period has a higher load due to space heating, and a tripled cost on MPGT compared to the summer, the MPGT cost is the highest during winter. The summer period amounted to only 20% of the total MPGT cost due to the low cost and low demand. With the high focus on keeping the peak-import level down in winter, this lessens the ability to shift electricity imports away from high-price peaks. Therefore, a cost decrease can be observed in Case 3 (SDP) for both the electricity cost and for MPGT, since the STES enables seasonal variation, and provides the possibility to lessen the import for thermal demand during winter. The MPGT cost for summer has increased by 42% in Case 3 (SDP) compared to Case 1 (SDP), which is primarily to fill the STES for the winter period. The impact is shown by decreasing the MPGT cost for winter, totaling at a 40.5% decrease from Case 1 (SDP). The overall MPGT cost reduction for the whole year is 23.9%, which is a substantial value for the overall cost reduction. Some electricity cost reduction is also seen between Case 1 (SDP) and 3 (SDP), although the overall import has increased to cover the thermal losses in the STES, demonstrating the flexibility in load shifting on a seasonal level through the STES.

4.3. SDP performance compared to perfect information

The SDP framework solves a decomposed optimisation problem that only contains known information 24 hours into the future. The rest of this horizon is projected through the EFCCs, which accounts for uncertainty in the stochastic variables. As such, the EFCCs promotes a future projection that tackles the uncertainty in the future, which changes how the MPGT and STES should account for all future projections of scenarios during operation. Additionally, having discrete values of the MPGT and STES in the EFCC can also lead to inaccuracies if the cost-optimal decision is between two discrete points. Due to these limitations of the SDP framework, comparing the performance to cases with perfect information provides insight into how much these inaccuracies influence operation, with the added value of having perfect foresight. The PI-instance, which keeps the 24-hour initial condition, can capture the improved performance if the discrete EFCC-representation was removed and we had perfect information, but still has restrictions as if decomposing the problem. The PI-instance without this initial condition manages to showcase the additional improved performance if the assumptions made to couple the decomposed problems were not needed.

Table 1 compares the average operational and economical performance of all cases and instances. This table includes performance on the STES in terms of maximum storage, and on the MPGT in terms of total cost due to highest peak of operation, allowing us to compare how the operational performance on the two state variables differ.

In general, the results showcase that there is limited differences in performance when comparing the use of SDP to the PI-instances. As

Table 1
Averaged operational and economic results of three cases, including the decomposed problems using SDP, and the cases with perfect information. (PI 24) keeps the 24-hour initial condition constraint, while (PI) does not consider it.

Case	Total Cost [EUR]	Max STES SoC [kWh]	Electricity Cost [EUR]	Grid tariff Cost [EUR]	MPGT Cost (Summer/Winter) [EUR]	Total Import [kWh]
Case 1 (SDP)	1336.2	0	686.1	650.1	209.5 (42.3/167.2)	13970.0
Case 1 (PI 24)	1335.2	0	686	649.2	208.6 (41.8/166.7)	13973.8
Case 1 (PI)	1310.7	0	683.7	627.0	188.3 (39.8/148.9)	13903.4
Case 2 (SDP)	2155.4	3257.5	635.4	1520	1070.0 (267.5/802.5)	14334.5
Case 2 (PI 24)	2154.7	3296.1	634.7	1520.0	1070.0 (267.5/802.5)	14336.3
Case 2 (PI)	2142.5	3214.6	624.3	1518.2	1070.0 (267.5/802.5)	14264.2
Case 3 (SDP)	1275.2	4560.3	663	612.2	159.4 (59.9/99.5)	14444.0
Case 3 (PI 24)	1273.7	4534.2	662.9	610.8	158.3 (59.4/98.9)	14430.8
Case 3 (PI)	1264.2	4494.2	657.8	606.4	156.1 (58.6/97.5)	14345.3

expected, both PI-instances have an improvement on total cost of operation over the year, and (PI) has the best performance. This is valid for all three cases. PI-instances for Case 1 see a decrease in both the cost of operation and MPGT cost. Case 1 (PI 24) has a 0.4% MPGT cost decrease, which is evenly distributed between summer and winter. These small cost changes come from knowing directly what peak to aim for during each month, and no discrete MPGT representation makes it possible to find the exact values to achieve. Case 1 (PI) has a 10.1% MPGT cost decrease compared to Case 1 (SDP), which mostly comes from the winter months. The increased flexibility for this PI-case enables more peak-shaving to reduce the load pattern during winter, which leads to a decrease in cost of operation by 1.9%. Overall, the benefit of SDP compared to the PI-cases is being able to find exact peak import levels for each month.

Case 2 focuses on operating the STES over the course of the year. For Case 2 (PI 24), the operational improvements give higher maximum STES SoC, and a lower total cost for the year of operation. The maximum STES SoC increased by 1.2% in Case 2 (PI 24), which demonstrates that the optimal strategy would be to store more thermal energy during the summer period. The discrete representation of the STES influences how accurate the projection of the marginal cost of increasing the STES SoC is, which would impact how much storage we deem it cost-effective to make use of. Additionally, as the thermal load for space heating is the stochastic variable of this case study, eliminating uncertainty would give more efficient use of the STES. For Case 2 (PI), the improved performance leads to the lowest STES SoC for Case 2 (SDP), alongside a lower cost of operation. This result shows that the STES has higher usage and SoC to account for the simplification on space heating demand, that the indoor temperature must be reset at the end of each operational day. Since only the STES would be influenced by the space heating indoor temperature and the initial condition, this does suggest that the initial conditions could have been adjusted to be more effective, which is supported by a decrease in total import. The STES SoC decreased by 1.3% compared to Case 2 (SDP), with a total cost reduction of 0.6%.

Case 3 incorporates both price signals. Case 3 (PI 24) has an overall decrease in cost of operation by 0.1% compared to Case 3 (SDP), showing marginal improvements on cost. However, the maximum STES SoC has decreased by 0.6%, and the overall cost decrease from MPGT is at 0.7%. Here, the optimal strategy with perfect information would mean that the STES would have lower SoC, and lower peaks during operation. For MPGT cost, the cost reduction is almost even between summer and winter, indicating that most of the reduction stems from a higher level of detail on the perfect peak level to aim for within each month. As the maximum STES SoC decreased, there was no strategic need to increase SoC to deal with thermal energy during winter, as was the case for Case 2 (SDP). This trend suggests that Case 3 (SDP) through the EFCCs emphasises the MPGT cost more, where the EFCCs would rather have higher STES SoC to ensure operation to handle the MPGT. This could be due to discretizing the EFCCs and the inaccuracy from that, and due to the thermal demand being the stochastic part, where the cost of having insufficient SoC uncertainty is harsher on the MPGT cost.

When ignoring the initial conditions in Case 3 (PI), the overall cost of operation decreases by 0.9%, with reductions in both STES SoC and MPGT cost. The MPGT cost decreases more in the winter period than the summer period, showing that the limitation influenced the most during winter with high thermal demand. The use of the STES in combination with the initial conditions for indoor temperature, as mentioned in Case 2 (SDP), seems to also occur here. Overall, the PI-instances result in small changes to economic performance compared to the SDP framework, showing only small decreases in cost of operation, MPGT cost, and use of STES.

The small changes to the economic performance do, however, create new strategic use of the STES in terms of the MPGT cost. Fig. 6 showcase the operational performance for all instances in Case 3 regarding MPGT peak levels and STES SoC, for the 50 percentile values. Here, there are some distinct observations that should be clarified. Overall, there are very small changes between Case 3 (SDP) and Case 3 (PI 24), in terms of both the peak levels and STES SoC. In general, Case 3 (SDP) with EFCCs perform close to optimal given the initial condition restriction, and the small deviations in operation are mostly due to discretisation of the state variables. Some areas do have different strategies, for instance in July where the peak level for the SDP case is a bit higher than both PI-instances.

However, the strategic use is somewhat different for the Case 3 (PI), which is free from the initial condition. Here, the peak levels have some

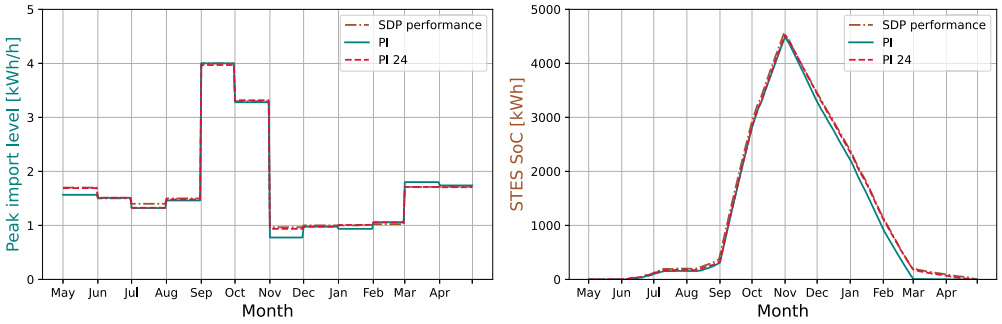

(a) Operational performance for MPGT peak levels

(b) Operational performance for STES SoC values

Fig. 6. Operational performance for all Case 3-instances. 50 percentiles are illustrated for all cases.

specific months with deviation, and the overall STES SoC is lower during the winter month. Overall, the strategy in Case 3 (PI) has changed: the STES are used more aggressively in the early months to lower the peak, leading to an almost empty STES from March. The peak level does increase in March as a result, but in general, the reduction in November and January makes it more cost-effective. Early use of the STES during winter results in less storage losses in the STES. For the two other cases, the STES has about 150 kWh of thermal energy stored for the last two months. Based on the findings in Case 3 (PI), this leftover energy is primarily used to handle the initial condition restrictions to avoid increasing the peak levels. This also makes it valuable for decreasing the peak level in March. This shows that despite the SDP case not being able to perform exactly optimal due to uncertainty and restrictions from decomposition, it is able to strategically adapt and benefit in other situations. Overall, despite this variation in use of the STES, the cost difference between Case 3 (SDP) and Case 3 (PI) is only 0.9%. These observations demonstrate that the SDP performance is able to capture how the MPGT and STES influence each other, despite some small improvements that could be made with perfect information.

Thermal demand for space heating was the only stochastic variable in this analysis, which did influence the strategic use of the STES and MPGT. The low amount of uncertainty does make the comparison to the PI-instances marginal, but it also showcases how the SDP methodology and the EFCCs manage to capture the strategy of the two state variables. The expected value of perfect information was limited if the assumptions for the SDP framework were kept, as shown for the (PI 24)-instances. When removing this assumption, the benefit increased, which proved that the primarily value-increase for this analysis revolved around this assumption. With increasing stochastic variables, the strategy would lead to more variations compared to the PI-instances, but would also enable us to capture what state variables are considered the most critical to account for with increasing uncertainty. The SDP methodology with EFCCs does manage to capture their dependencies, which is valuable for making long-term operational decisions with multiple signals to account for.

5. Conclusion

We have presented a long-term strategic modelling framework for operational planning within a flexible building, with the aim of operating seasonal flexibility optimally over the year. With the use of stochastic dynamic programming (SDP), the future value of operation is represented by future cost curves generated for two different state variables at the same time. This analysis has considered seasonal thermal energy storage (STES) and a monthly measured-peak grid tariff (MPGT) as long-term price signals that are represented in the future cost curves. Moreover, the SDP framework has been extended in order to update the recurring monthly MPGT cost in the operational strategy for each month during the year. During this update, it is vital that the yearly strategy for the STES is kept to promote the long-term strategy, which will also contain information on how the future demand charge costs influence the strategy surrounding seasonal storage.

The framework has been applied to a realistic Norwegian single-family house located in the Norwegian bidding zone NO2 for the year 2019, with an available STES and MPGT cost over the year. Just considering the MPGT cost lead to decreasing peak import levels during the year, but seasonal variations in load lead to higher levels during winter. By only accounting for the STES, it is filled during late summer to make use of the spot-price variations between the seasons. When both price signals are included, the strategy made more cost-effective decisions to lower cost of operation. The STES state-of-charge came up higher during summer, accomplished by increasing the peak-import during summer, which in turn led to significant peak-import reduction during winter. The overall operational strategy of the STES was to provide stable thermal energy during winter, while uncertainty in thermal demand was mostly covered by the electrical side during operation. The yearly cost saving from MPGT is 23.9% higher compared to having no STES installed, with a total cost reduction of 4.3%. Additionally, the performance was compared to simulations with perfect information, which showcased a 0.1% total cost improvement with constraints similar to a decomposed problem, and a 0.9% cost improvement without these constraints. This showcases that the SDP framework is able to capture the long-term strategy regarding both the MPGT and STES similarly to operational planning under perfect foresight. Even though the long-term future is uncertain in our case study, the SDP framework produces close to optimal decisions here-and-now towards the long-term uncertain future.

This long-term strategy could be built upon in future work. For instance, it could be applied to larger energy systems like neighbourhoods to investigate large-scale use of flexibility. New long-term flexibility markets, like fast-frequency reserves in Norway where load reduction is reserved for parts of the summer season, could be incorporated within the SDP framework. This would allow to investigate how much flexibility to sell, and the consequence of operation during non-optimal flexibility volume offers. Additionally, investigating the long-term strategy influence considering a system-perspective on the energy system can open new views on how to best make use of the flexibility within end-users for grid-based support. Further, we encourage further work to compare the energy flows resulting from linear state-space models in techno-economic optimization models with energy flows resulting from more advanced building simulation and/or measured data.

CRediT authorship contribution statement

Kasper Emil Thorvaldsen: Writing – original draft, Visualization, Validation, Software, Methodology, Investigation, Formal analysis, Data curation, Conceptualization. **Stian Backe:** Writing – original draft, Supervision, Project administration, Funding acquisition, Formal analysis. **Hossein Farahmand:** Writing – original draft, Supervision, Investigation, Funding acquisition, Formal analysis.

Declaration of competing interest

The authors declare that they have no known competing financial interests or personal relationships that could have appeared to influence the work reported in this paper.

Data availability

The authors do not have permission to share data.

Acknowledgements

This work was funded and supported by the Research Council of Norway and several partners through FME ZEN (Grant Number: 257660/E20) and FME CINELDI (Grant Number: 257626/E20). The authors gratefully acknowledge the financial support from the Research Council of Norway and all partners in FME CINELDI and FME ZEN. Thanks to Salman Zaferanlouei at NTNU for lending computational performance to run the cases in this work. Also, thanks to Magnus Korpås at NTNU for feedback on the paper.

Appendix A. EFCCs for Case 1 and Case 2

In the following, a more detailed description of the EFCCs for the SDP-instances of Case 1 and Case 2 will be given. As the overall focus of this work was to look at the coupling of multiple state variables, the detailed description of each state variable independently is given here.

A.1. Case 1 - only measured peak grid tariff

The cost curves generated in Case 1 only account for peak import costs within the SDP Framework. The EFCCs describe the increase in the cost of operation within each month when increasing the highest single-hour import of electricity.

The marginal EFCC for Case 1 is shown in Fig. A.7, including the cost curves for both a summer and winter day. The change in marginal EFCC describe how the highest peak import influence strategic operation in terms of cost. For lower peak import values, the marginal cost increase stays at 0, indicating that this threshold is not economically or technically feasible to keep during the month, promoting higher peaks during operation. Likewise, at the highest peak import values, the marginal cost is close or equal to the marginal cost of the MPGT for the given month. This is due to any increase in peak import only affecting the MPGT cost, not giving any additional benefits during operation. For any values between 0 and the MPGT cost, the strategy implies that the peak can be increased, with some future cost increase, but what is lower than the MPGT cost. This is due to increased benefits in terms of more load shifting capabilities towards spot-price variation or other flexible benefits. Additionally, uncertainty also plays a role, given by the weighted cost in the curves. For increasing peak import, the additional benefits from load shifting decrease, causing the net marginal cost increase to approach the MPGT cost.

Comparing the strategic peak import for both summer and winter in Fig. A.7, the most distinct difference between the two cost curves is the initial value of peak import, where the marginal cost is non-zero. For the summer day, the non-zero value initiates around 1.5 kWh/h, and around 2.0 kWh/h for the winter day. This is influenced by the electric demand, which increases during winter to cover the thermal load from colder outdoor temperature. This increased load makes it either not feasible or economically optimal to uphold the import lower than 2.0 kWh/h for this specific month. Due to the high thermal demand, it is possible that the technical limit could be below 2.0 kWh/h, but that the additional cost from flattening the load and thus import during high spot-price hours exceeds the savings from the MPGT cost. Additionally, the slope of both curves are very different, motivated by the different seasonal marginal cost. The MPGT cost during summer is three times lower than during winter, making peak-shaving during winter more cost-effective than during summer. This also showcases a potential additional value by the introduction of seasonal storage, which could make it possible to increase load during summer, and thus increase the MPGT cost, to reduce the load during winter, and reduce the winter MPGT cost. Therefore, the seasonal variation in MPGT cost promotes peak shifting between the seasons.

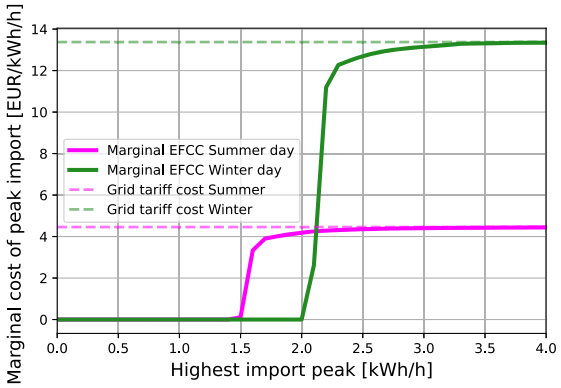

Fig. A.7. Plot of the marginal EFCC for only the MPGT in Case 1, for both the summer and winter day.

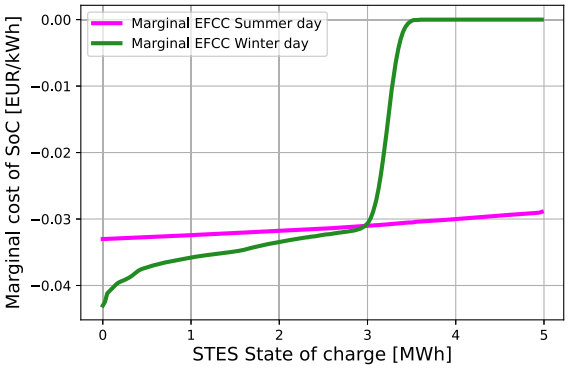

Fig. A.8. Plot of the marginal EFCC for only the SoC of the STES in Case 2, for both the summer and winter day.

A.2. Case 2 - only seasonal storage

Case 2 generates cost curves that capture the future value of altering the STES SoC during operation. This includes the whole year of operation, meaning that the future value of increasing SoC considers the marginally costliest unit that would be covered in the future by this increase, which would normally be covered by electricity. Since the only source of thermal energy is electricity, spot-price variation between summer and winter acts as the motivation storing energy between the two seasons. The marginal EFCC for Case 2 is depicted in Fig. A.8, which includes both a summer and winter day. The cost of operation is negative, since an increase in SoC decrease the future need to import electricity. Therefore, the cost is negative, showcasing a future value for the STES SoC. In general, both the winter and summer day projects a decreasing value (less negative) for higher SoC on the STES.

With the SDP framework, the marginal value is linked to the future situation of thermal load. For the winter period, which can only discharge, the marginal value depends on if it is cost-optimal to discharge the thermal load now, or store it for future use. For the lowest SoC, the benefit is the highest, since that would cover the marginally costliest thermal energy in the future period. For large SoC, the marginal value approaches 0, which indicates that reaching these storage levels would provide more thermal storage than we need to cover in the future. For the summer period, which can only charge the STES, the

marginal value depends on whether the marginal unit could be stored in a future summer month at a more cost-optimal price, but also the cost that this marginal unit would replace during the winter period. The benefit is decreasing slowly with increasing SoC, but does not reach a 0 marginal value. This suggest that there is not large price-variation for the future, and also that one could fully charge the storage unit without exceeding the thermal demand during winter. Therefore, these marginal values gives a continuous overview over the future value of storing more thermal load, and does a comparison to the here-and-now prices for producing this marginal unit of thermal energy.

It is very noticeable that there are different trends and behaviours between the winter and summer period in Fig. A.8. Since the winter day only considers the future planning of discharging the existing thermal energy, the value is varying to a larger degree and also has a 0 marginal value for large SoC. The variation in electricity price is the main factor for the spread of values. But it does show that for low SoC, the benefit increases enough to showcase that the strategy would be to distribute the remaining energy for hours of need. The strategy for the summer period in the summer day is much different, due to not only planning the SoC needed for the winter period, but also whether or not to store more energy now or later during the summer period. However, the spot-price variation is not that large for this specific day. This suggests that the opportunity to store thermal energy is available for the hours with low spot-price. Therefore, depending on the spot-price variation in this setting, it would either not consider it (spot-price is too high), would periodically store electricity (spot-price variation is around threshold), or continuously store (spot-price is below). As such, the cost curves for both periods show different strategies on use of the STES, to make use of the seasonal storage capabilities in a cost-optimal manner.

References

[1] S. Vitiello, N. Andreadou, M. Ardelean, G. Fulli, Smart metering roll-out in Europe: where do we stand? Cost benefit analyses in the clean energy package and research trends in the green deal, Energies 15 (7) (2022) 2340, https://doi.org/10.3390/EN15072340, https://www.mdpi.com/1996-1073/15/7/2340/htm.

[2] Norges vassdrags- og energidirektorat, Forslag til endring i forskrift om kontroll av nettvirksomhet, Tech. Rep., 2017, www.nve.no.

[3] K. Rune Verlo, B. Araberg Fladen, A. Meling og Urd Sira, Oppsummering av høring og anbefaling til endringer i nettleiestrukturen Reguleringsmyndigheten for energi-RME, www.nve.no.

[4] Nettleiepriser 2019 - Agder Energi Nett, https://www.aenett.no/globalassets/publikasjoner/nettleiepriser-2019-privat.pdf, 2019.

[5] Agder Energi | AE.no, https://www.ae.no/.

[6] ACER Report on Distribution Tariff Methodologies in Europe, https://documents.acer.europa.eu/Official_documents/Acts_of_the_Agency/Publication/ACER_Report_on_D-Tariff_Methodologies.pdf, 2021.

[7] L. Xu, S. Wang, F. Xiao, An adaptive optimal monthly peak building demand limiting strategy considering load uncertainty, Appl. Energy 253 (2019) 113582, https://doi.org/10.1016/J.APENERGY.2019.113582.

[8] L. Xu, H. Tang, S. Wang, Adaptive optimal monthly peak building demand limiting strategy based on exploration-exploitation tradeoff, Autom. Constr. 119 (2020) 103349, https://doi.org/10.1016/J.AUTCON.2020.103349.

[9] F. Luo, W. Kong, G. Ranzi, Z.Y. Dong, Optimal home energy management system with demand charge tariff and appliance operational dependencies, IEEE Trans. Smart Grid 11 (1) (2020) 4–14, https://doi.org/10.1109/TSG.2019.2915679.

[10] K. Emil Thorvaldsen, S. Bjarghov, H. Farahmand, Representing long-term impact of residential building energy management using stochastic dynamic programming, in: 2020 International Conference on Probabilistic Methods Applied to Power Systems (PMAPS), IEEE, 2020, pp. 1–7, https://ieeexplore.ieee.org/document/9183623/.

[11] A. Hesaraki, S. Holmberg, F. Haghighat, Seasonal thermal energy storage with heat pumps and low temperatures in building projects—a comparative review, Renew. Sustain. Energy Rev. 43 (2015) 1199–1213, https://doi.org/10.1016/J.RSER.2014.12.002.

[12] S.K. Shah, L. Aye, B. Rismanchi, Seasonal thermal energy storage system for cold climate zones: a review of recent developments, Renew. Sustain. Energy Rev. 97 (2018) 38–49, https://doi.org/10.1016/J.RSER.2018.08.025.

[13] R. Renaldi, D. Friedrich, Techno-economic analysis of a solar district heating system with seasonal thermal storage in the UK, Appl. Energy 236 (2019) 388–400, https://doi.org/10.1016/J.APENERGY.2018.11.030.

[14] B. McDaniel, D. Kosanovic, Modeling of combined heat and power plant performance with seasonal thermal energy storage, J. Energy Storage 7 (2016) 13–23, https://doi.org/10.1016/J.EST.2016.04.006.

[15] T. Brown, D. Schlachtberger, A. Kies, S. Schramm, M. Greiner, Synergies of sector coupling and transmission reinforcement in a cost-optimised, highly renewable European energy system, Energy 160 (2018) 720–739, https://doi.org/10.1016/J.ENERGY.2018.06.222.

[16] R. Egging-Bratseth, H. Kauko, B.R. Knudsen, S.A. Bakke, A. Ettayebi, I.R. Haufe, Seasonal storage and demand side management in district heating systems with demand uncertainty, Appl. Energy 285 (2021) 116392, https://doi.org/10.1016/j.apenergy.2020.116392.

[17] M. Jokiel, D. Rohde, H. Kauko, H.T. Walnum, Integration of a High-Temperature Borehole Thermal Energy Storage in a Local Heating Grid for a Neighborhood, 2020, pp. 31–38, pp. 13–14, https://sintef.brage.unit.no/sintef-xmlui/handle/11250/2683179.

[18] C. Kang, C. Chen, J. Wang, An efficient linearization method for long-term operation of cascaded hydropower reservoirs, Water Resour. Manag. 32 (10) (2018) 3391–3404, https://doi.org/10.1007/s11269-018-1997-2.

[19] L.E. Schäffer, A. Helseth, M. Korpås, A stochastic dynamic programming model for hydropower scheduling with state-dependent maximum discharge constraints, Renew. Energy 194 (2022) 571–581, https://doi.org/10.1016/J.RENENE.2022.05.106.

[20] M. Saadat, K. Asghari, Reliability improved stochastic dynamic programming for reservoir operation optimization, Water Resour. Manag. 31 (2017) 1795–1807.

[21] R. Bellman, A Markovian Decision Process, 1957.

[22] V.N. Gudivada, D. Rao, V.V. Raghavan, Big Data Driven Natural Language Processing Research and Applications, Handbook of Statistics, vol. 33, Elsevier, 2015, pp. 203–238.

[23] K.E. Thorvaldsen, S. Bjarghov, H. Farahmand, Representing Long-Term Impact of Residential Building Energy Management Using Stochastic Dynamic Programming, 2020.

[24] R.C. Sonderegger, Dynamic models of house heating based on equivalent thermal parameters, Ph.D. Thesis, 1978.

[25] P. Bacher, H. Madsen, Identifying suitable models for the heat dynamics of buildings, Energy Build. 43 (7) (2011) 1511–1522, https://doi.org/10.1016/j.enbuild.2011.02.005.

[26] B. Cui, C. Fan, J. Munk, N. Mao, F. Xiao, J. Dong, T. Kuruganti, A hybrid building thermal modeling approach for predicting temperatures in typical, detached, two-story houses, Appl. Energy 236 (2019) 101–116, https://doi.org/10.1016/J.APENERGY.2018.11.077.

[27] J. Salpakari, T. Rasku, J. Lindgren, P.D. Lund, Flexibility of electric vehicles and space heating in net zero energy houses: an optimal control model with thermal dynamics and battery degradation, Appl. Energy 190 (2017) 800–812, https://doi.org/10.1016/j.apenergy.2017.01.005.

[28] Y. Zhang, P.E. Campana, Y. Yang, B. Stridh, A. Lundblad, J. Yan, Energy flexibility from the consumer: integrating local electricity and heat supplies in a building, Appl. Energy 223 (2018) 430–442, https://doi.org/10.1016/j.apenergy.2018.04.041.

[29] Ringerikskraft, https://www.ringerikskraft.no/.

[30] V. Lakshmanan, S. Bjarghov, P. Olivella-Rosell, P. Lloret-Gallego, I. Munné-Collado, M. Korpås, Value of flexibility according to the perspective of distribution system operators — a case study with a real-life example for a Norwegian scenario, A working paper.

[31] sonnenBatterie, https://sonnengroup.com.

[32] M. Jafari, M. Korpås, A. Botterud, Power system decarbonization: impacts of energy storage duration and interannual renewables variability, Renew. Energy 156 (2020) 1171–1185, https://doi.org/10.1016/j.renene.2020.04.144.

[33] ZEB Living Lab., https://www.zeb.no, https://www.zeb.no/index.php/en/pilot-projects/158-living-lab-trondheim.

[34] P.J.C. Vogler-Finck, J. Clauß, L. Georges, I. Sartori, R. Wisniewski, Inverse Model Identification of the Thermal Dynamics of a Norwegian Zero Emission House, Springer, Cham, 2019, pp. 533–543.

[35] M. Berge, H.M. Mathisen, Perceived and measured indoor climate conditions in high-performance residential buildings, Energy Build. 127 (2016) 1057–1073, https://doi.org/10.1016/j.enbuild.2016.06.061.

[36] SINTEF energy research KMB project 190780/S60, ElDeK, electricity demand knowledge, https://www.sintef.no/en/projects/eldek-electricity-demand-knowledge/.

[37] New tariffs from 2022 - Lnett., https://www.l-nett.no/nynettleie/new-tariffs-from-2022.

[38] Nord Pool, https://www.nordpoolgroup.com.

[39] Renewables.ninja, https://www.renewables.ninja/.

[40] MERRA-2, https://gmao.gsfc.nasa.gov/reanalysis/MERRA-2/.

[41] Pyomo, http://www.pyomo.org/.